Chapter 3

Testing of the SPH Code

To test the SPH code, a variety of simulations are performed and compared to analytic calculations or results from other numerical methods. In Section 3.1, the hydrodynamic elements of the code are tested by shock tube calculations. Sections 3.2 to 3.4 contain calculations that check both the hydrodynamic and gravitational elements of the code. In all cases, particular interest is taken in the role and behaviour of the SPH code's artificial viscosity (Equations 2.31 and 2.32).

3.1 Shocks and Particle Interpenetration

The artificial viscosity used in the SPH code is required to reproduce shock phenomena correctly and also to stop particle interpenetration. Particle interpenetration occurs, for example, when particles pass through a shock front without attaining the correct velocity and other physical quantities (see Figure 3.10). If particle interpenetration is not stopped then any particular position in the simulation may have multiple physical quantities which is not physical and results in poor reproduction of shocks. The standard artificial viscosity used in SPH has two parameters α and β. The α-viscosity provides a bulk viscosity, while the β-viscosity is used to stop particle interpenetration at high Mach numbers. Many authors have performed a variety of shock tests to find values of these parameters that accurately reproduce the shocks. It is generally agreed that α and β should have values of order unity, and $\alpha = 1$ and $\beta = 2$ are commonly recommended (Monaghan 1992), though the exact values required to most accurately reproduce shocks have been found to depend on the particular situation and cannot be generalised.

A calculation performed by Monaghan, and later by Heller, (Monaghan 1989; Heller 1991) allows us to investigate both the ability of SPH to model shocks and the problem of interpenetration of particles. The test is a one-dimensional problem with an analytic solution that the SPH results can easily be compared to. The initial state consists of an ideal gas $p = (\gamma - 1)\rho u$, with uniform density ρ_0, internal energy u_0, and pressure p_0, but with the velocity of the gas being discontinuous across the origin such that the gas is in two streams, one with negative coordinates and one with positive coordinates, travelling directly toward one another, each with speed v_0. The system evolves with the streams of gas colliding at the origin producing a stationary shocked region with density ρ_1, internal energy u_1, and pressure p_1, and two shock waves propagating outward from the origin with speed v relative to the rest frame, as more gas continues to collide with the shocked gas.

Monaghan and Heller both perform the test using an adiabatic equation of state. Here two equations of state are used. First an adiabatic equation of state with $\gamma = 5/3$ and adiabatic sound speed $c_s = \sqrt{\gamma p/\rho}$, and second, an isothermal equation of state with isothermal sound speed $c_s = \sqrt{p/\rho}$. Analytic solutions can be found for both these cases using the Hugoniot shock relations (Zel'dovich & Raizer 1966). Using the dimensionless system of units where $\rho_0 = 1$, $p_0 = 1$ we find that for the adiabatic case where $u_0 = 1/(\gamma - 1)$ and $c_s = \sqrt{\gamma}$ the analytic solution is

$$v = \frac{(\gamma-3)v_0 + \sqrt{(\gamma+1)^2 v_0^2 + 16\gamma}}{4}, \tag{3.1}$$

$$\frac{\rho_1}{\rho_0} = 1 + \frac{v_0}{v}, \tag{3.2}$$

$$\frac{u_1}{u_0} = \frac{\rho_0}{\rho_1} + v_0 v, \tag{3.3}$$

$$\frac{p_1}{p_0} = 1 + v_0(v + v_0), \tag{3.4}$$

For the isothermal case ($\gamma = 1$), with $\rho_0 = 1$, $p_0 = 1$, and $c_s = 1$, the analytic solution is

$$v = \frac{-v_0 + \sqrt{v_0^2 + 4}}{2}, \tag{3.5}$$

$$\frac{\rho_1}{\rho_0} = \frac{p_1}{p_0} = 1 + \frac{v_0}{v}. \tag{3.6}$$

These tests are performed with one, two and three-dimensional versions of the SPH code to gain information about what viscosity parameter values are needed to accurately model shocks and stop particle interpenetration in all three dimensions and to see what, if any, are the problems in going from one to higher dimensions.

3.1.1 Initial Particle Distributions

Three different initial distributions of particles are used for the shock tests performed in more than one dimension to see if the initial distribution significantly affects the results. In one dimension, the particles are evenly spaced along the x-axis with the origin falling half-way between two particles. In two and three dimensions the particles are initially placed in a grid pattern in a box. Three different patterns are used. All of these allow perfect, reflective, ghost-particle boundaries (or periodic boundaries) to be used to contain the gas. The particles' ghosts are formed by reflecting the positions of real particles through the boundaries so the distribution of ghosts is identical to the real particles and forms a continuation of the grid. This allows a relatively small number

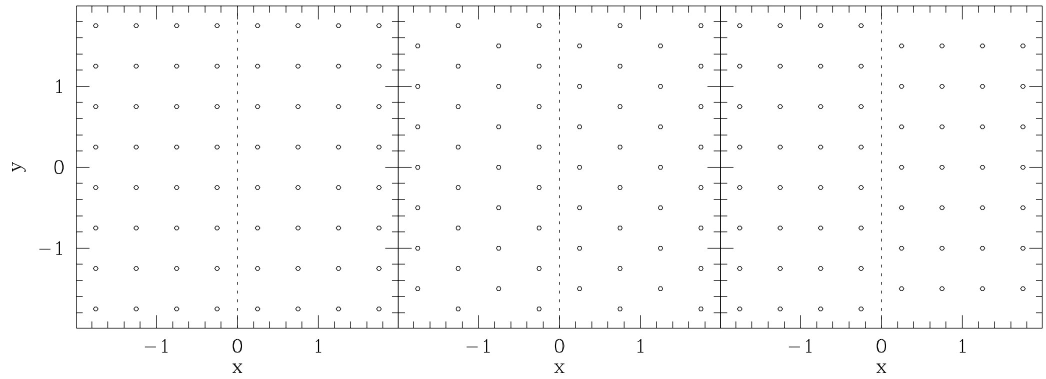

Figure 3.1: The three different initial particle distributions used in the two-dimensional SPH shock simulations. They are cubic lattice (left), unaligned lattice (centre) and offset lattice (right). The three-dimensional SPH distributions are the three-dimensional equivalent. Motion is parallel to the x-axis.

of real particles to be used in the simulations, and higher resolution can be obtained with less computational time than if the boundaries had to be far from the origin so as not to affect the area of interest. The three distributions are shown, as used in the two-dimensional tests, in Figure 3.1. In three dimensions the patterns used are the three-dimensional equivalent. The simplest distribution is a cubic (square) lattice. The second distribution is similar to the cubic lattice, except that every second set of particles along the x-axis is displaced along the y-axis (and z-axis in three dimensions) by half the interparticle spacing so that consecutive particles along the x-axis are unaligned. We call this the unaligned lattice. The final pattern is specifically for the investigation of particle interpenetration and has two cubic lattices, which are offset from each other along the y-axis (and z-axis in three dimensions) at the origin of the x-axis - a column of particles in one stream faces the hole in-between columns of the opposing stream. It is expected that the cubic lattice should give the best results as particles are all aligned with each other at the shock, so interpenetration should be least likely, and it is similar to many one-dimensional calculations together. The unaligned lattice is used to be more like a typical SPH distribution of particles, to see if the lack of alignment makes any difference to the results. The offset distribution should be the worst possible case with respect to particle interpenetration occurring at the initial shock point, as particles should be able to stream through the gaps opposite them on the other side of the origin relatively easily.

3.1.2 Reproduction of the Shock

The first simulations study the differences between the reproduction of the shock in one, two and three-dimensional SPH simulations. The shock test is done adiabatically with $v_0 = c_{\rm s}$ so that the relative collision speed of the two streams is twice the initial sound speed. Note that at this collision speed both the α-viscosity and β-viscosity are important. Figure 3.2 shows the one-dimensional result, and the two and three-

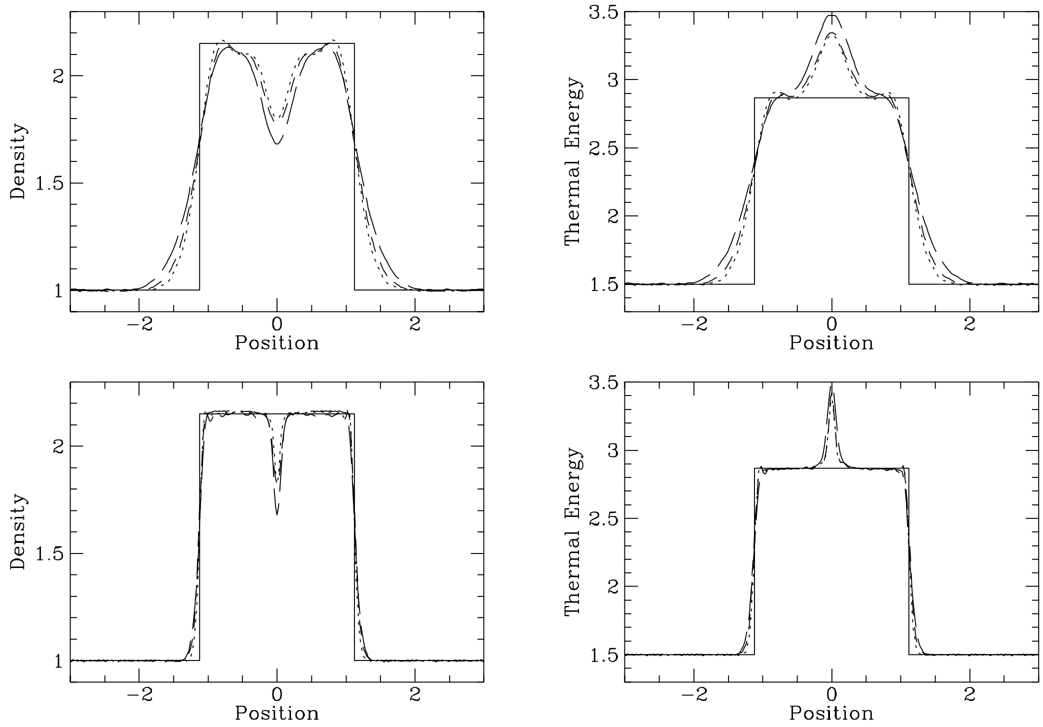

Figure 3.2: Adiabatic shock test at $t = 1$ with $v_0 = c_s$ performed in one (long dashed), two (dashed) and three (dotted) dimensions and with two different x-axis particle resolutions of 4 (top) and 16 (bottom) particles per unit length. The simulations have artificial viscosity of $\alpha = 1$ and $\beta = 2$ and use the cubic lattice distribution. The solid line is the analytic result.

dimensional results using the cubic lattice distribution, with high and low-resolution calculations. These are compared to the analytic result at time $t = 1$. The higher resolution SPH simulations reproduce the shock well, with the speed of the shock wave being correctly simulated and the density of the shocked gas being correct to $\leq 1\%$ and the thermal energy being correct to $\leq 0.3\%$. The differences from the analytic result come from the lack of resolution and the effects of the initial velocity discontinuity. First, the shock edge is smoothed out over approximately three smoothing lengths ($3h$). In the low-resolution calculation, this leads to the whole shock being smoothed out, while with high resolution only the edges are affected. The second observation is that the thermal energy is over estimated at the origin, leading to an underestimate in the density. This was described by Monaghan as the 'wall effect'. It comes from the fact that the initial conditions are discontinuous in velocity at the origin, and particles there initially collide at twice v_0, while later on, particles entering the shock front are only travelling at v_0 relative to the shocked gas. This gives the extra heating at the origin which is also spread over $\approx 3h$, and so decreases in width as the resolution increases, as the particles within this region are the only ones to see particles travelling at $2v_0$ relative to them. The 'wall effect' can be eliminated if the initial velocity discontinuity is smoothed over several smoothing lengths, however if this is done, the problem of particle interpenetration in

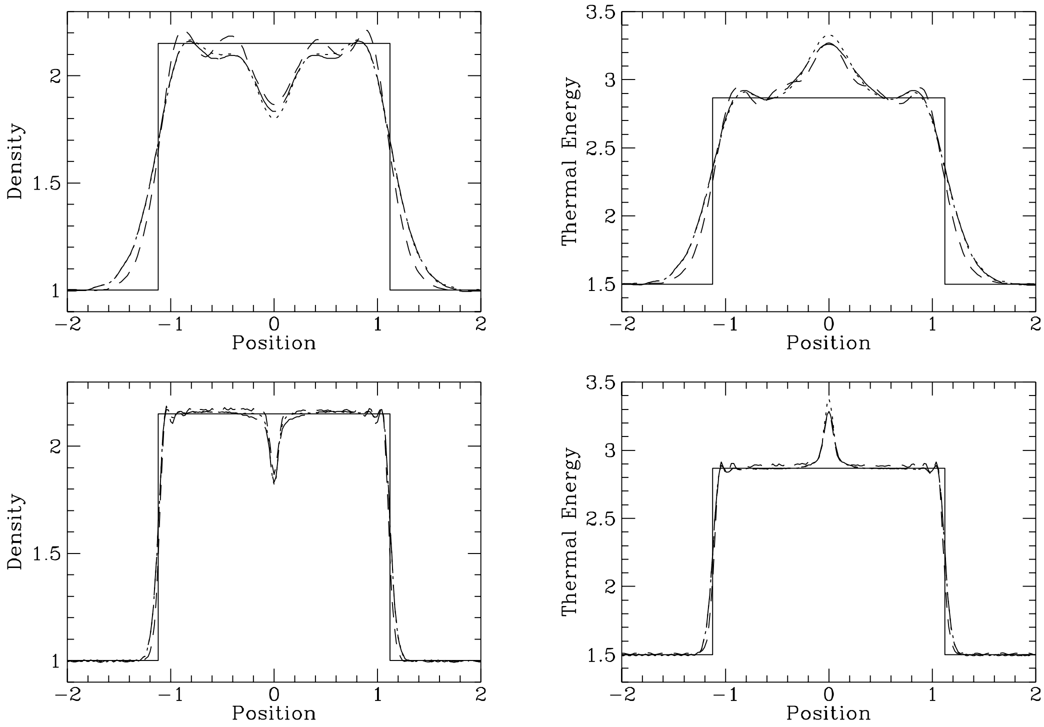

Figure 3.3: Adiabatic shock test at $t = 1$ with $v_0 = c_s$ performed in three dimensions with two different x-axis particle resolutions of 4 (top) and 16 (bottom) particles per unit length, each with the three different distributions, cubic (dotted), unaligned (dashed), and offset (long dashed). The artificial viscosity is $\alpha = 1$ and $\beta = 2$. The solid line is the analytic result.

SPH cannot be studied (see Section 3.1.3). Finally, note that there is some difference between the shock profiles in different dimensions. This is mainly because different smoothing lengths are being used in different dimensions to keep the correct number of neighbours, and thus the smoothing of the shock differs slightly.

Figure 3.3 shows the results of three-dimensional calculations with low and high resolution and with cubic, unaligned, and offset lattice distributions. The differences between the cubic and offset lattice results are negligible as they are both based on a cubic lattice, and the viscosity is such that particle interpenetration does not occur. There are minor differences between the cubic and unaligned lattice results. The shock edge is spread over a smaller distance in the unaligned calculation than the cubic lattice. This is because the particle smoothing lengths can be slightly smaller with the unaligned lattice than the cubic lattice and still contain the required number of neighbours, so the resolution is slightly increased.

From Figures 3.2 and 3.3 then, we observe that reproduction of the shock is not very dependent upon the particle distribution or dimension of the simulation, assuming the particle distribution is relatively uniform in all directions and significant particle interpenetration does not occur (see Section 3.1.3). Instead it depends mainly upon the resolution due to the smoothing lengths of the particles.

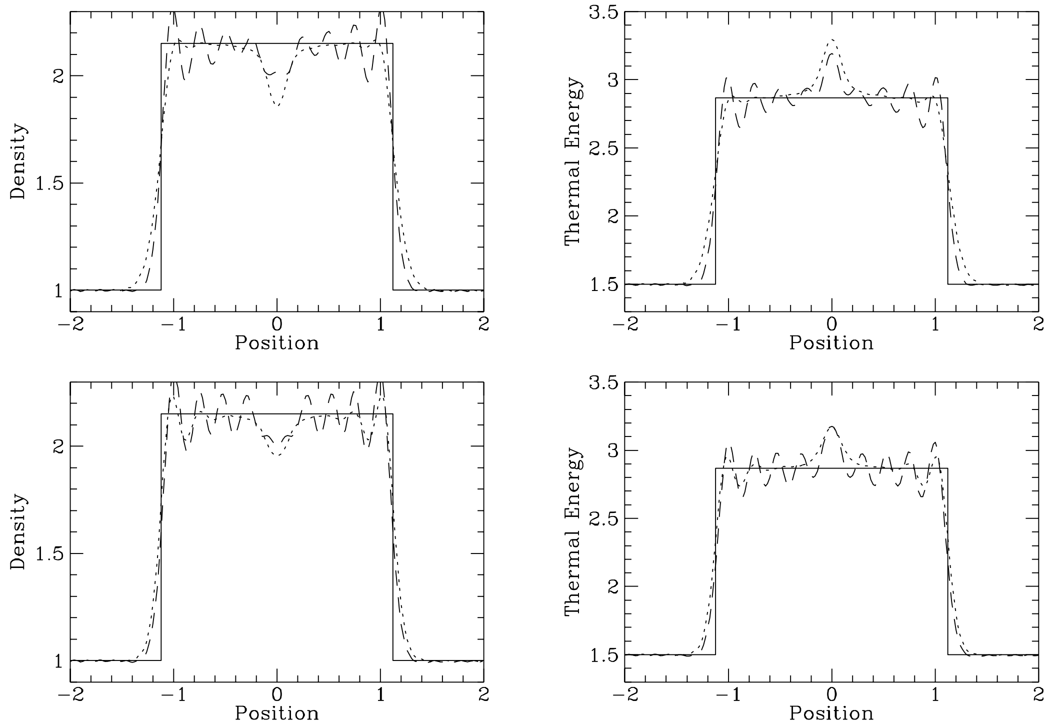

Figure 3.4: Adiabatic shock tests at $t = 1$ with $v_0 = c_s$ performed in three dimensions with the offset particle distribution and varying viscosity. The top graphs show the effect of reducing the total viscosity from $\alpha = 1$ and $\beta = 2$ (dotted) to $\alpha = 0.4$ and $\beta = 0.8$ (dashed). The bottom graphs demonstrate the effect of having only one type of viscosity, with either $\alpha = 1$ and $\beta = 0$ (dotted), or $\alpha = 0$ and $\beta = 2$ (dashed). The particle resolution is 8 particles per unit length. The solid line is the analytic result.

We now vary the artificial viscosity to observe the effect of low and high viscosity and how the α-viscosity and β-viscosity differ in their affect (Figure 3.4). The general trends shown by these calculations are independent of particle distribution, though again details do differ. Notice that the low viscosity calculation has sharper edges on the shock than the higher viscosity calculation. As stated earlier, with $\alpha = 1$ and $\beta = 2$ the shock edge is spread over $\approx 3h$, but this value is dependent on the viscosity and increases with increased viscosity. With low viscosity ($\alpha = 0.4$, $\beta = 0.8$), the shock is well reproduced globally, but large oscillations in density and internal energy appear in the shocked region. The lack of viscosity allows particles to oscillate behind the shock (see Figure 3.6 for examples of particle velocity oscillation along the shock). It can be broken down into two main effects. The result with only α-viscosity used has very little oscillation within the shock, but significant oscillation at the edge. The β-viscosity result has large oscillation all along the shock. This shows the regions where the α-viscosity and β-viscosity are active. The α-viscosity is needed to provide bulk viscosity within the shock to eliminate post-shock, subsonic oscillations, while the β-viscosity is needed at the shock edge to prevent particle interpenetration or near interpenetration when the

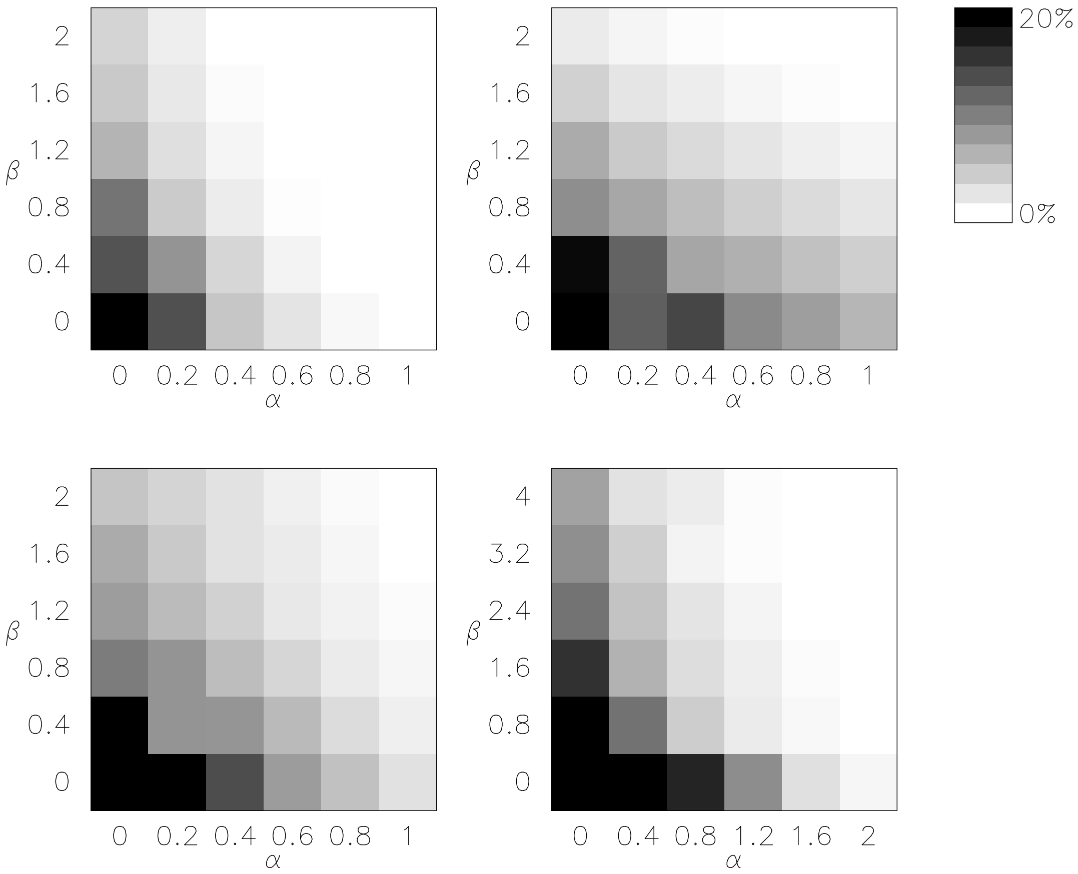

Figure 3.5: The root-mean-square velocity dispersion of particles in the adiabatic shock, as a percentage of the initial sound speed, at $t = 1$ with varying α and β. The calculations are performed with $v_0 = c_s$ in one (upper-left), two (upper-right) and three (lower-left) dimensions, and with $v_0 = 4c_s$ in two dimensions (lower-right). The particle resolution is 8 particles per unit length and the offset particle distribution is used.

particles have relative velocities of order the sound speed or higher. The $\alpha = 1$ and $\beta = 2$ result is well behaved with very little oscillation in the shocked region.

In different dimensions, there is a dependence on the values of the viscosity needed to produce similar results. This can be seen in Figure 3.5 which gives the root-mean-square particle velocities as a percentage of the initial sound speed in the shocked region of gas. Generally, higher viscosity is needed for higher-dimension simulations, as particles find it easier to oscillate or interpenetrate in higher dimensions due to their lack of alignment with each other. Also, in one dimension all viscous forces from neighbouring particles act directly against the oscillation, whereas with higher dimensions, many particles in the SPH kernel barely contribute to the viscous force on an oscillating particle as their positions are perpendicular to the direction of oscillation, and hence the mean viscous force is reduced. The different effects of the α-viscosity and β-viscosity are also apparent in the grey-scale plots. It is clear from the one-dimensional result that α-viscosity is more effective than β-viscosity at reducing post-shock oscillation, which is

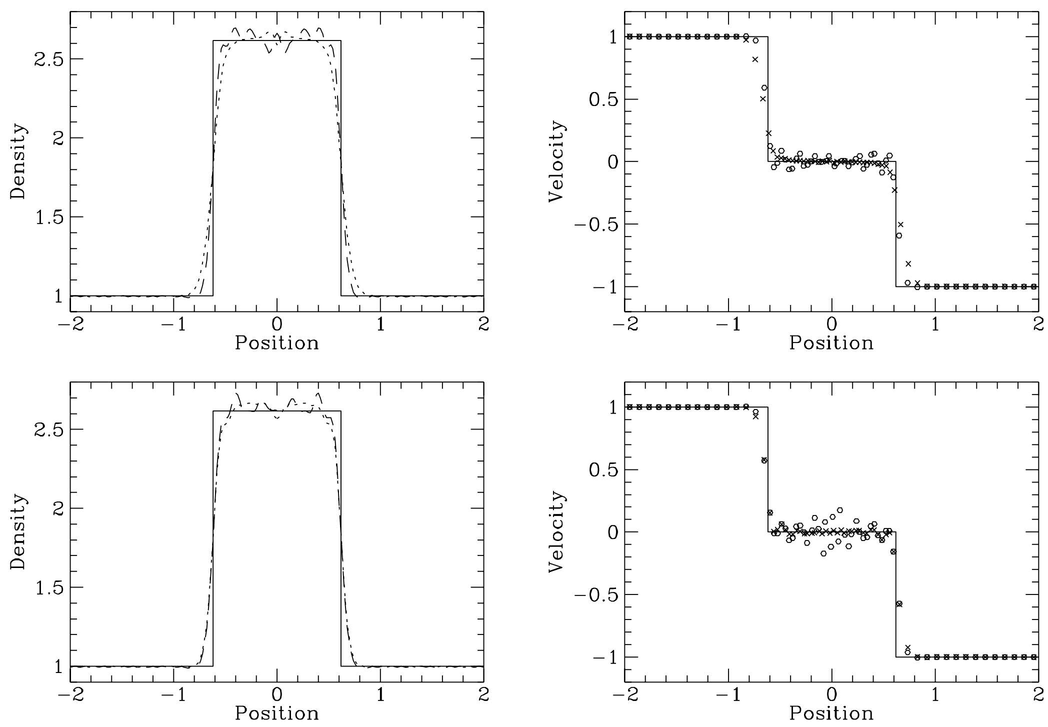

Figure 3.6: Isothermal shock tests at $t = 1$ with $v_0 = c_s$ performed in three dimensions with the offset particle distribution and varying viscosity. Density and particle velocities are given. The top graphs show the effect of reducing the viscosity from $\alpha = 1$ and $\beta = 2$ (dotted, crosses) to $\alpha = 0.4$ and $\beta = 0.8$ (dashed, circles). The bottom graphs demonstrate the effect of having only one type of viscosity, with either $\alpha = 1$ and $\beta = 0$ (dotted, crosses), or $\alpha = 0$ and $\beta = 2$ (dashed, circles). The particle resolution is 11 particles per unit length. The solid line is the analytic result.

as expected as it is supposed to act as a bulk viscosity and from its formulation is the dominant viscous force at subsonic velocities. This is less clear in the two and three-dimensional simulations as these use the offset particle distributions for which significant particle interpenetration occurs in some of the lower viscosity calculations. The particle interpenetration increases the dispersion of velocities along the shock in these cases. Cases where significant particle interpenetration occurred can be found by comparing Figures 3.5 and 3.11. When the shock velocity is very supersonic (as in the $v_0 = 4c_s$ case where the relative shock speed is Mach 8), it becomes very evident that α-viscosity is the dominant mechanism for reducing post-shock oscillation, and β-viscosity alone is ineffective. Finally, we note that in two and three dimensions with velocities near the sound speed, similar results can be obtained with each of the viscosities separately if α is replaced by $\beta \sim 2\alpha$, though the details differ. This reflects the fact that at Mach $\sim$ 1 both viscosities have a significant effect, and the higher value of β relative to α is due to the fact that the effect of the β-viscosity diminishes as the velocity decreases whereas with the α-viscosity it does not.

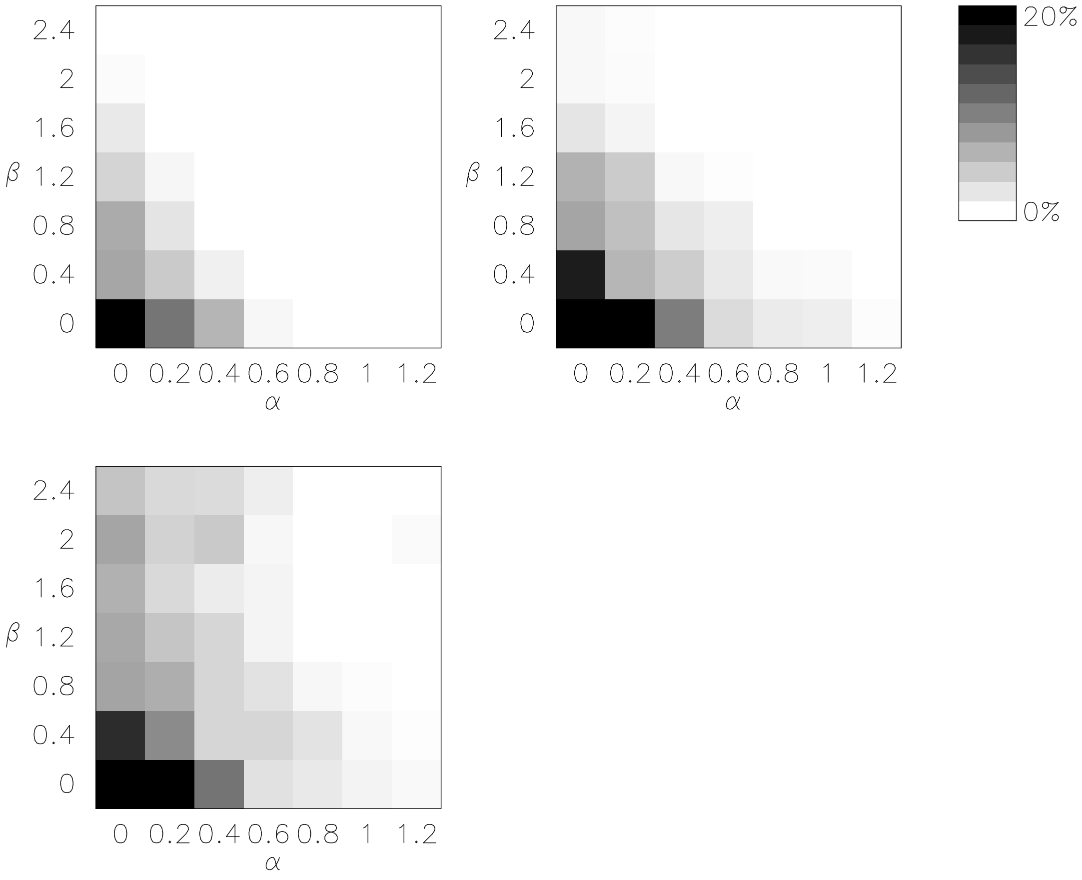

Figure 3.7: The root-mean-square velocity dispersion of particles in an isothermal shock, as a percentage of the sound speed, at $t = 1$ with varying α and β. The calculations are performed with $v_0 = c_s$ in one (upper-left), two (upper-right) and three (lower-left) dimensions. A calculation with $v_0 = 4c_s$ is not shown as dramatic particle interpenetration occurs for all values of the viscosity (see Section 3.1.3). The offset particle distribution is used with a particle resolution of 8 particles per unit length.

We now consider isothermal shocks. Again there is little difference between SPH in different dimensions and with different particle distributions, so long as the particle distribution remains fairly uniform and particle interpenetration is stopped. Isothermal shocks with $v_0 = c_s$ are shown in Figure 3.6. The most obvious difference between these and the adiabatic shocks is that the 'wall effect' does not occur as the gas is isothermal and hence over-heating at the initial velocity discontinuity does not occur. The effect of different viscosities on the post-shock particle oscillation is the same, with the particle velocities themselves being plotted. Again the absence of α-viscosity leads to large subsonic velocity oscillations whereas the absence of β-viscosity only has an effect at the edges of the shock where the relative velocities of particles are large. With $\alpha = 1$ and $\beta = 2$ the shock is well treated, with very little velocity and density dispersion along the shock. The fact that α-viscosity is more effective in reducing particle velocity dispersion within the shocked region is again demonstrated in Figure 3.7 (which can be compared

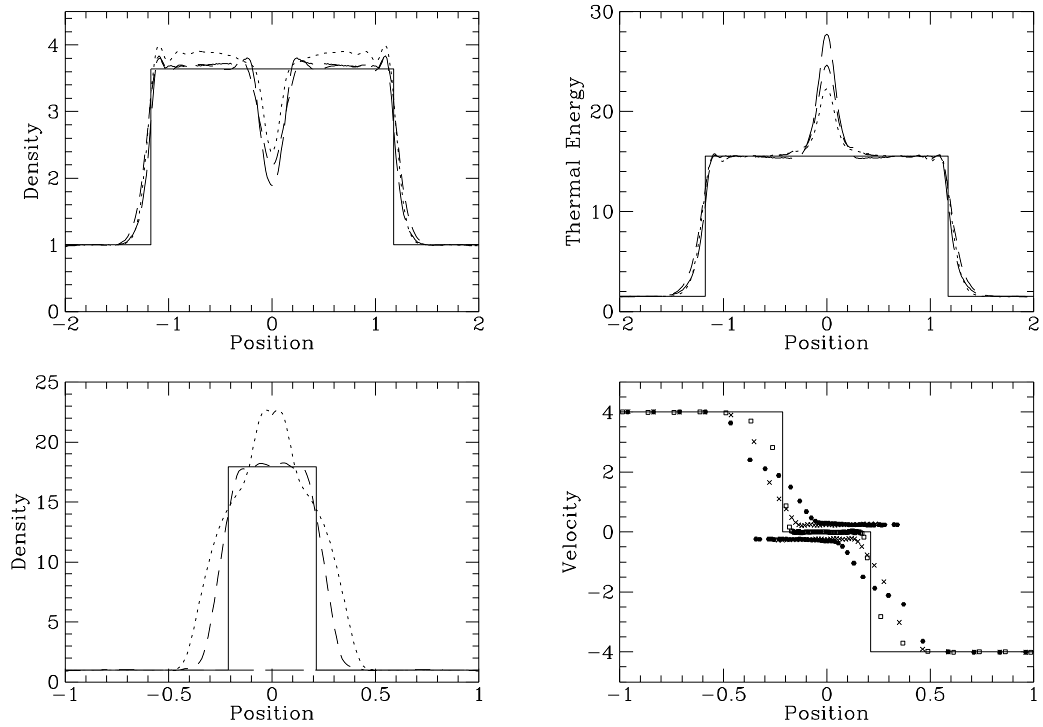

Figure 3.8: Adiabatic (top) and isothermal (bottom) shock tests at $t = 1$ and $t = 0.6$ respectively. The shock speed is $v_0 = 4c_\mathrm{s}$ and results for one (long-dashed, squares), two (dashed, crosses), and three (dotted, circles) dimensional calculations are given. The viscosity is $\alpha = 1$ and $\beta = 2$ and the particle distribution is the offset distribution with a resolution of 8 particles per unit length. The solid line is the analytic result.

to Figure 3.12 to see where particle interpenetration effects are important).

Finally, we look at high-Mach-number shocks, as up to now most analysis has been done with $v_0 = c_\mathrm{s}$ and hence a relative shock speed of Mach 2. Figure 3.8 gives the results of shock simulations with $v_0 = 4c_\mathrm{s}$ (i.e. relative shock speed of Mach 8) with adiabatic and isothermal equations of state using one, two and three-dimensional versions of SPH. The offset particle distribution is used and viscosity is $\alpha = 1$ and $\beta = 2$. The adiabatic shock has an even larger 'wall effect' than the slower shocks, which is expected. Other than the 'wall effect', the thermal energy in the shock is well reproduced, and in the one and two-dimensional cases the density is also well reproduced. However, in the three-dimensional calculation, the density is over estimated by The reason for this is the variable-smoothing-length, spherical kernel that is being used. The shocked gas has 3.62 times the original density. Since the shock test is a one-dimensional problem, this higher density is attained by compressing the particle distribution along the axis of motion. The particle distribution used here is the offset distribution, which if particle interpenetration is stopped (as it is here) means that the particles are compressed along lines. As this happens, the particles' kernels shrink to retain the same number of neighbours, and eventually they start to become 'detached' from the neighbouring

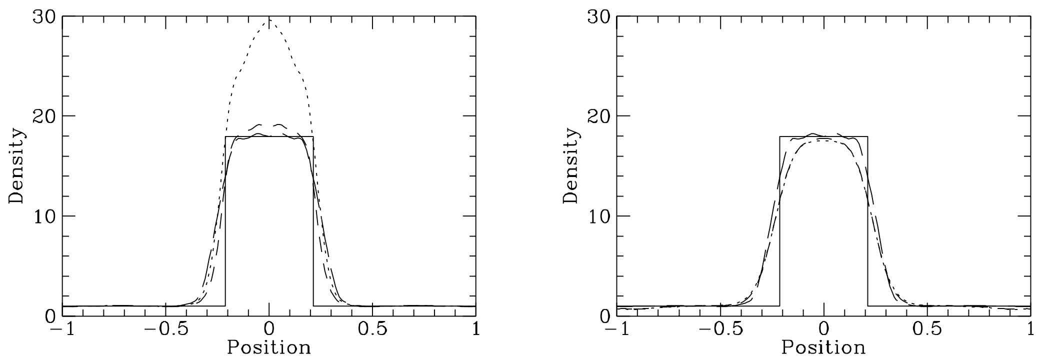

Figure 3.9: Isothermal shock tests at $t = 0.6$ with $v_0 = 4c_s$ performed in two dimensions with the cubic (dotted), unaligned (dashed) and offset (long-dashed) particle distributions. The calculations on the left have variable smoothing lengths, whereas those on the right have constant smoothing lengths equal to the initial particle spacing (h=0.125). The viscosity is $\alpha = 1$ and $\beta = 2$ and the particle resolution 8 particles per unit length. The solid line is the analytic result.

particle streams. When this occurs, the density of the fluid is being calculated from a one-dimensional distribution of particles, but using a three-dimensional kernel. This leads to an over-estimate of the shock density. The effect is even more dramatic in the isothermal shock, as the correct density of the shock is now 17.94 times the original density and the particles are strongly compressed.

This over-estimate of the density is, of course, strongly dependent on the particle distribution as is shown by the two-dimensional calculations in Figure 3.9. Here the three different particle distributions are used with variable and constant smoothing lengths. The cubic distribution is worst as the particles are all in lines. However, even the unaligned particle distribution shows a density over-estimate as the distribution is being compressed so drastically along one dimension. The reason the offset distribution shows no density over-estimate, is due to particle interpenetration which reduces the separation between the particle streams and they do not become detached. This can be seen by the particle velocity plots in Figure 3.8. In both the two and three-dimensional cases, the viscosity does not stop particle interpenetration occurring throughout the shock region. This leads to the incorrect reproduction of the width of the shock in the two and three-dimensional isothermal calculations in Figure 3.8, as shocked particles are not stopped and flow right through the shock! The calculations done with constant smoothing lengths in Figure 3.9 show no density over-estimate, as the kernels are large enough to always sample a two-dimensional particle distribution. In addition, the results from cubic and unaligned calculations are virtually identical as particle interpenetration is stopped in both of them. Some particle interpenetration does occur with the offset particle distribution and this gives the slightly broader shock density as compared to the other constant-smoothing-length calculations.

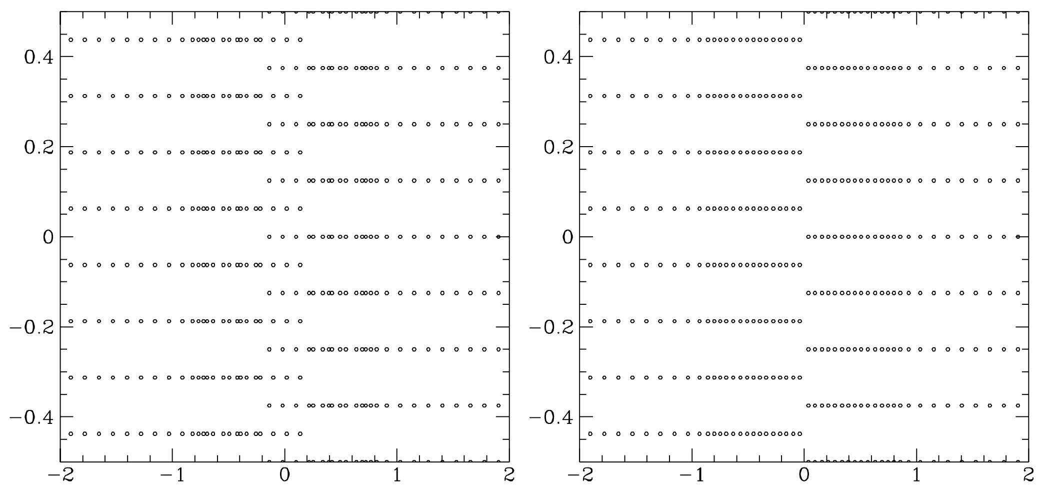

Figure 3.10: Particle distributions from a two-dimensional adiabatic shock test with $v_0 = c_s$ using the offset particle distribution at time $t = 0.8$ where particle interpenetration occurs using $\alpha = 0.2$ and $\beta = 0.4$ (left) and where it is stopped by artificial viscosity of $\alpha = 0.6$ and $\beta = 1.2$ (right). A constant particle smoothing length equal to the initial particle spacing is used.

3.1.3 Particle Interpenetration

The problem of particle interpenetration in SPH is a complicated one, with several factors contributing to whether or not particle interpenetration occurs. It depends upon the number of dimensions of the calculation, the particle distribution, the relative velocities of the particles, the smoothing lengths of the particles, the equation of state, and, of course, the magnitude and type of artificial viscosity used. Each of these factors is looked at in turn. Initially all calculations are performed with constant particle smoothing lengths. Later, results with variable smoothing lengths are given, but initially it is important to use constant smoothing lengths so that different effects may be isolated.

First we investigate how particle interpenetration differs as the α and β parameters are varied. An example of particle interpenetration across the shock interface is given in Figure 3.10. In the first case, three layers of particles along the x-axis have been penetrated by particles from the first layer of the opposing stream. In the second case, the viscosity is sufficient to stop particle interpenetration from occurring.

Figure 3.11 shows how many layers of particles along the x-axis are penetrated by the first layer of the opposing stream before they are stopped for simulations calculated with different values of α and β. The adiabatic equation of state is used. The two and three-dimensional calculations use the offset particle distribution, as, of the three dimensions, it is expected that this will allow the most interpenetration to occur. It is evident that as the number of dimensions increase, more artificial viscosity is required to ensure there is no particle interpenetration. Also for calculations with $v_0 = c_s$, both α-viscosity and β-viscosity can effectively stop particle interpenetration, since as was seen in the previous section both viscosities are important at velocities of around Mach 1. Again

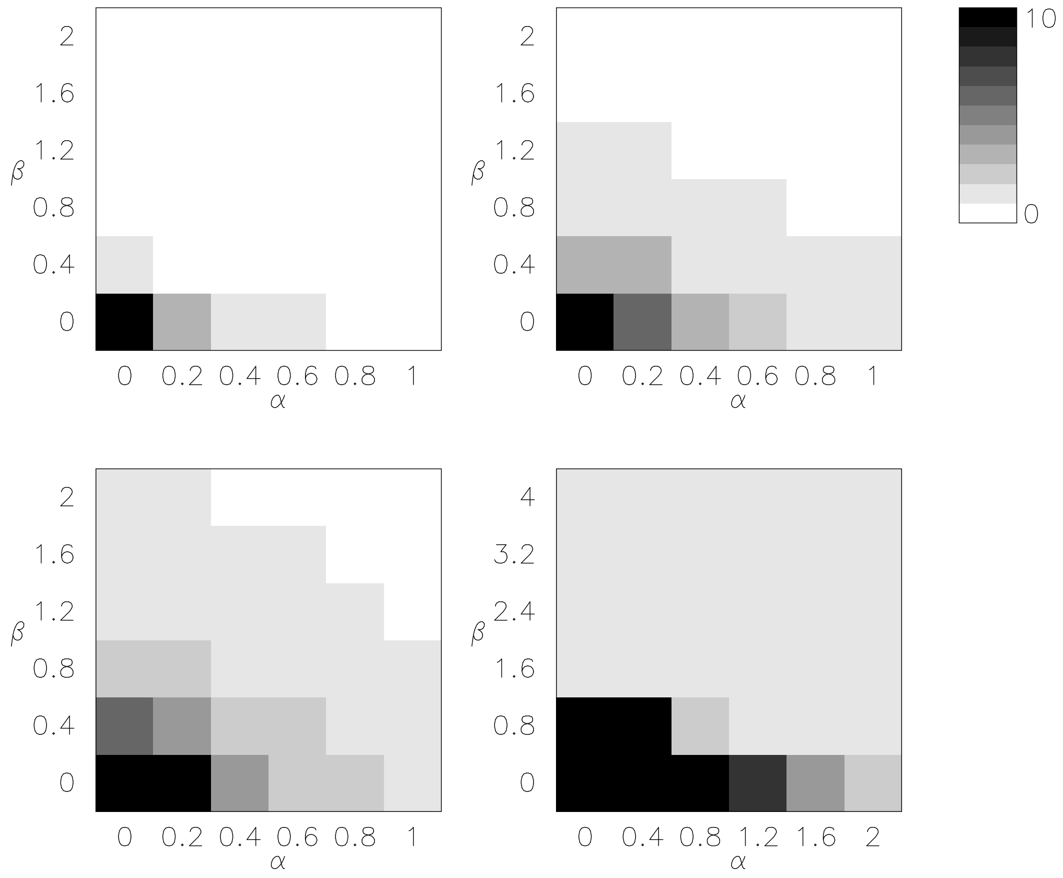

Figure 3.11: Number of layers of the opposing stream of particles through which the the first layer of particles penetrates before the penetration is halted. The adiabatic equation of state is used with α and β varied. The calculations are performed with $v_0 = c_s$ in one (upper-left), two (upper-right) and three (lower-left) dimensions, and with $v_0 = 4c_s$ in two dimensions (lower-right). The offset particle distribution is used, with the smoothing lengths of the particles kept constant at the initial particle spacing ($h = 0.125$).

though, this varies with the relative shock speed as demonstrated by the calculations with $v_0 = 4c_s$, in which β-viscosity is more effective than α-viscosity in stopping particle interpenetration. This $v_0 = 4c_s$ case is slightly misleading as it implies no value of the viscosity is enough to stop penetration completely. In fact for most of the cases in Figure 3.11 where the penetration is restricted to the first layer, although penetration does occur, the particles 'bounce' back to a final state where they have not penetrated.

Figure 3.12 shows the same thing, but using the isothermal equation of state. Here higher overall viscosity is needed to stop particle interpenetration compared to the adiabatic shocks. This is because in the adiabatic case the shocked gas is heated, increasing its sound speed, which effectively increases the α-viscosity (Equation 2.31). A second reason is that particles are being 'pushed' through the shocks. This is discussed below.

In the most of the remainder of this section, we set $\beta = 2\alpha$ to reduce the parameter

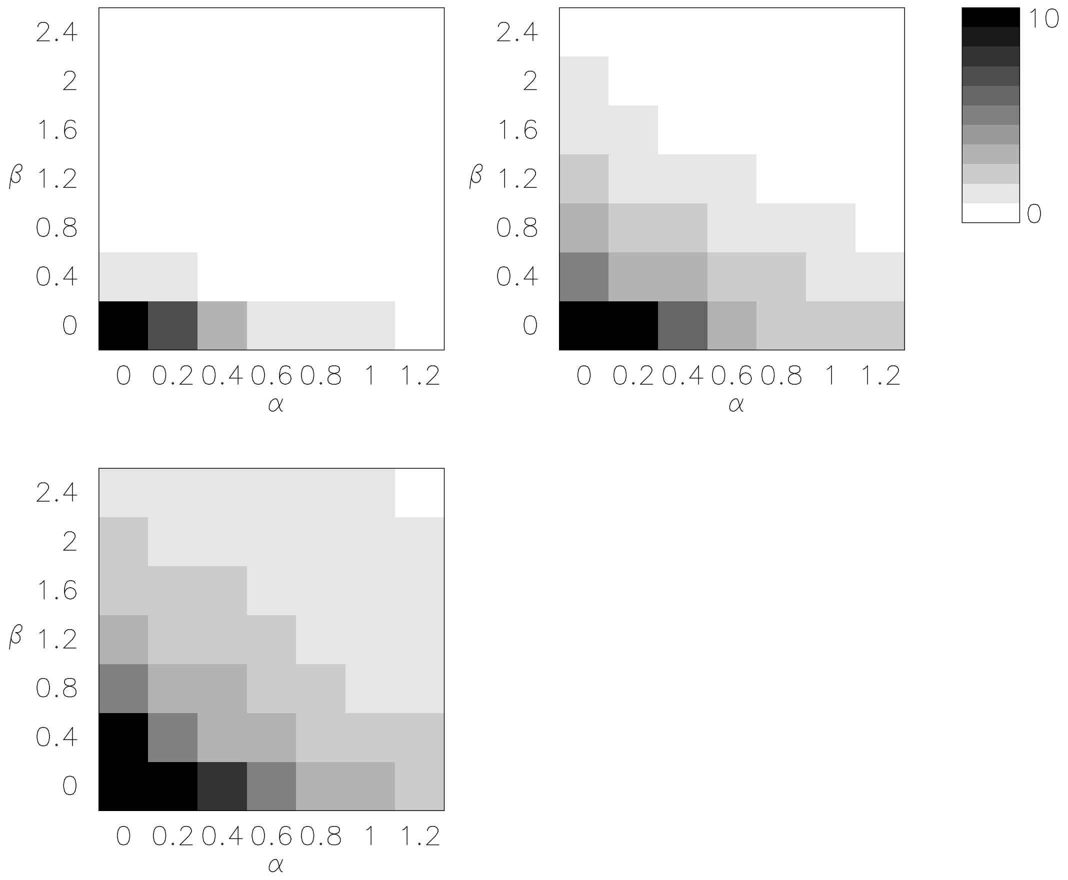

Figure 3.12: Number of layers of the opposing stream of particles through which the the first layer of particles penetrates before the penetration is halted. The isothermal equation of state is used with α and β varied. The calculations are performed with $v_0 = c_\mathrm{s}$ in one (upper-left), two (upper-right) and three (lower-left) dimensions. A calculation with $v_0 = 4c_\mathrm{s}$ is not shown as particle penetration is not stopped for any value of the viscosity but is on going through many layers (> 10). The offset particle distribution is used, with the smoothing lengths of the particles kept constant at the initial particle spacing ($h = 0.125$).

space of the problem of particle interpenetration. This parameterisation is chosen since for particle velocities of approximately the sound speed, Section 3.1.2 and Figures 3.11 and 3.12 show that α-viscosity and β-viscosity give similar results if $\beta \sim 2\alpha$ is used in the two and three-dimensional versions of the code. For high-Mach-number shocks, the β-viscosity does most of the work in stopping particle interpenetration and therefore it is the value of β that is most critical.

We now ask what values of the viscosity are required to stop particle interpenetration for various Mach number shocks in different numbers of dimensions. We define particle interpenetration not to have occurred if particles from the first layers of each of the opposing streams do not flow through the opposing layer before their initial motion has been halted or reversed. Note that in some cases this allows particle interpenetration to occur **after** this criterion has been fulfilled. It is possible for certain values

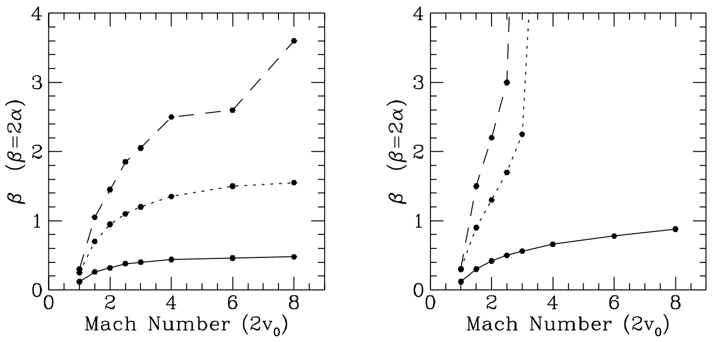

Figure 3.13: Value of β required to stop particle interpenetration from occurring with the parameterization $\beta = 2\alpha$ for various Mach number shocks. Shown are the adiabatic (left) and isothermal (right) shock results, in one (solid), two (dotted) and three (dashed) dimensions. All have a constant smoothing length equal to the initial particle spacing ($h = 0.125$). The offset particle distribution is used.

of α and β to be sufficient to stop initial particle interpenetration, but as will be seen below, the distributions of the particles after the shock can allow particles to be forced to interpenetrate, with velocities less than the sound speed, by pressure forces alone.

The values of α and β (with $\beta = 2\alpha$) needed to stop particle interpenetration with different Mach number shocks in each dimension are shown in Figure 3.13. As shown earlier, the isothermal calculations require more artificial viscosity to stop particle interpenetration than the adiabatic calculations. Also, the amount of viscosity needed to stop interpenetration increases with the relative Mach number of the two streams. Note that as the Mach number increases, it is the β-viscosity that is having most of the effect even though we still have $\beta = 2\alpha$. In the calculations performed in one dimension, the viscosity required increases slower with increasing Mach number, so that viscosity of $\alpha = 0.25$ and $\beta = 0.5$ is enough to stop particle interpenetration in the adiabatic shock with any relative speed less or equal to Mach 8. This general leveling-off of the required viscosity occurs for the adiabatic shocks in all three dimensions.

With the isothermal shocks, however, the leveling-off of the viscosity occurs only in the one-dimensional calculations. In two dimensions, above Mach 3 there is no value of the viscosity able to halt particle interpenetration and a similar problem occurs in three dimensions even earlier. The reason for this behaviour is the particle distribution. Because all motion is in one direction, the high density region of shocked gas is created by decreasing the particle separation along the x-axis. In adiabatic shocks, the density of the shocked gas has a limiting value of $\rho/\rho_0 = (\gamma+1)/(\gamma-1) = 4$ so the problem is less pronounced. But for isothermal shocks there is no such limiting density. As the Mach number of the isothermal shock increases, the density increases and the particles are forced closer together along the x-axis. With the offset particle distribution, there comes a point when the majority of the neighbours of the particle at the interface of the shock are particles from the same stream, and these particles dominate the pressure

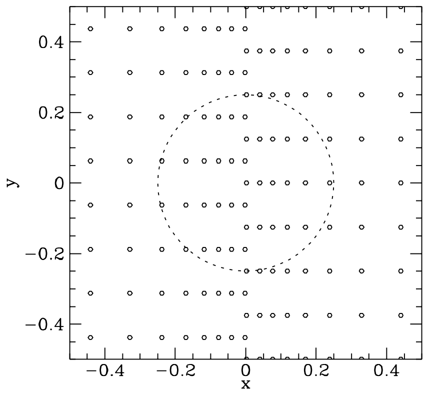

Figure 3.14: A typical particle distribution which allows the leading layer of one stream of particles to be forced, by pressure forces from its neighbours behind it and in the same stream, to penetrate the opposing stream of particles. The dotted circle marks out the kernel size for the particles ($2h$). This figure is from an isothermal shock test in two dimensions with constant smoothing length of the initial particle spacing with $\alpha = 1.9$ and $\beta = 3.8$ at $t = 0.25$, just before particle interpenetration starts to occur.

forces on the particle pushing it forward to penetrate the opposing layer regardless of the viscosity used. This is shown in Figure 3.14. This problem cannot be avoided while using spherical SPH kernels, though the use of particle velocity smoothing as suggested by Monaghan (1989) may improve the situation.

In a typical SPH simulation, the offset particle distribution should never occur, and thus the problem of particles being pushed through shocks by their neighbours should not be as severe. Figure 3.15 shows the adiabatic and isothermal results for two dimensions, for all three particle distributions and with two different smoothing lengths. For the cubic and unaligned lattice distributions the problem of particles being pushed through shocks by their neighbours does not occur (though glitches are still seen in the unaligned distribution results). As expected, the cubic lattice distribution requires the least amount of viscosity to stop interpenetration, as particles are all aligned and so should be stopped most easily, while the unaligned distribution, which is intended to be closer to what would be found in a typical SPH calculation, requires viscosities between the extremes of the cubic lattice and offset distributions.

From Figure 3.15 we also see that the size of the particle smoothing lengths affects the amount of viscosity required. Increasing the smoothing length relative to the particle spacing means that the viscosity must also be increased to stop particle interpenetration. This can be understood by considering that the viscosity acts over the distance scale, h, and so if h is increased, the viscosity must be increased since it is now required to stop the particles' motion over a smaller fraction of the distance h. The effect of changing the smoothing length is particularly dramatic in low Mach number shocks, with a major increase in the viscosity required.

In all the two-dimensional cases from Figure 3.15, $\alpha = 1$ and $\beta = 2$ is sufficient

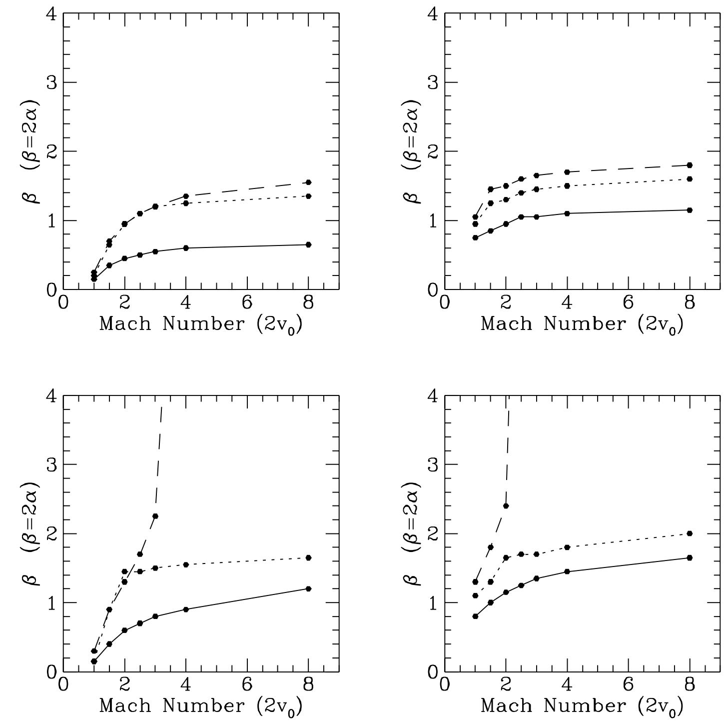

Figure 3.15: Value of β required to stop particle interpenetration from occurring with the parameterization $\beta = 2\alpha$ for various Mach number shocks. Shown are the adiabatic (top) and isothermal (bottom) shock results, with cubic (solid), unaligned (dotted) and offset (dashed) particle distributions and with constant smoothing lengths of 1 (left) and 1.5 (right) times the initial particle spacing ($h = 0.125$).

to stop particle interpenetration, except in cases where the problem of particles being pushed through the shock by pressure occur. Particles are pushed through the shock by pressure forces only in the isothermal shocks when the offset particle distribution is used and the Mach number is greater than 2.

We now present results of calculations where the code uses variable smoothing lengths (Figure 3.16). The general trends just discussed still apply, except that now the affect of particles being pushed through the shock in the cases with the offset distribution is even more pronounced. It now occurs with high-Mach-number adiabatic shocks as well as isothermal shocks. This is because as the densities increase in the shocked gas, the smoothing lengths of the particles reduce to maintain the same number of neighbours. The point is quickly reached, where the smoothing lengths become so small that most of their neighbours are particles from the same stream, and these push the leading particles through the shock interface. No value of viscosity can stop this penetration from occurring, as the particles are pushed through by pressure forces. Allowing particles to vary their smoothing lengths lets this occur even more easily than with constant smoothing lengths. Again this problem is due to the use of a spherical kernel, but this time even the use of velocity smoothing of particles would not help, as the kernel,

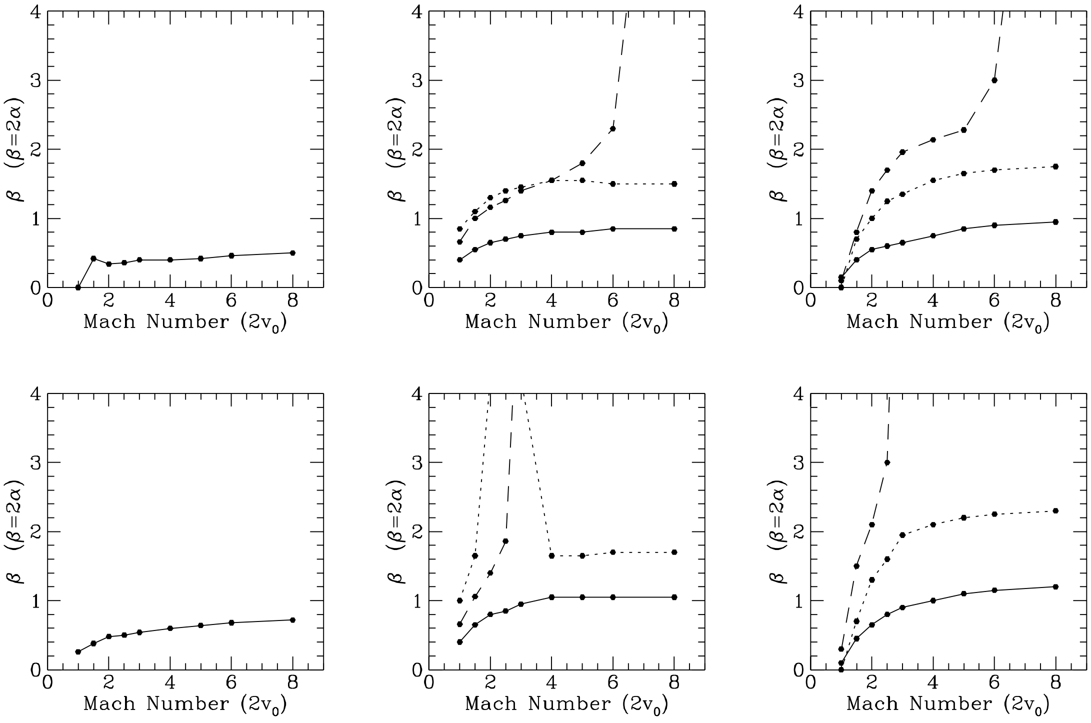

Figure 3.16: Value of β required to stop particle interpenetration from occurring with the parameterization $\beta = 2\alpha$ for various Mach number shocks. Shown are the adiabatic (top) and isothermal (bottom) shock results, with cubic (solid), unaligned (dotted) and offset (dashed) particle distributions in one (left), two (centre) and three (right) dimensions. The smoothing lengths of the particles are allowed to vary.

and hence the region over which the velocity smoothing is done, shrinks in size. This problem also occurs over a brief range of Mach numbers in the isothermal tests with the unaligned two-dimensional distribution where the particle positions happen to allow the problem to occur. In this case, however, the particles do not penetrate through more than the first layer, and often 'bounce' back later in the simulation, whereas with the offset distribution interpenetration may be continuous.

The offset particle distribution should never be allowed to occur in a typical SPH simulation, and the distribution of particles should be more like the unaligned distribution. Hence in general, a viscosity of $\alpha = 1$ and $\beta = 2$ in two dimensions, and $\alpha = 1.2$ and $\beta = 2.4$ in three dimensions, or higher, should be sufficient to stop most particle interpenetration in shocks with speeds of up to Mach 8 and using equations of state with $\gamma \gtrsim 1$. For higher Mach numbers, the required viscosity increases, though only gradually as can be seen from Figures 3.15 to 3.17.

The above calculations all assume the relation $\beta = 2\alpha$, and in many cases the use of this relation means that a value of $\alpha \ll 1$ is used when particle interpenetration is halted. The use of $\alpha \ll 1$ means that large velocity oscillations in can occur in the shocked gas however, and should not be used in practice. From Section 3.1.2 we know that $\alpha = 1$

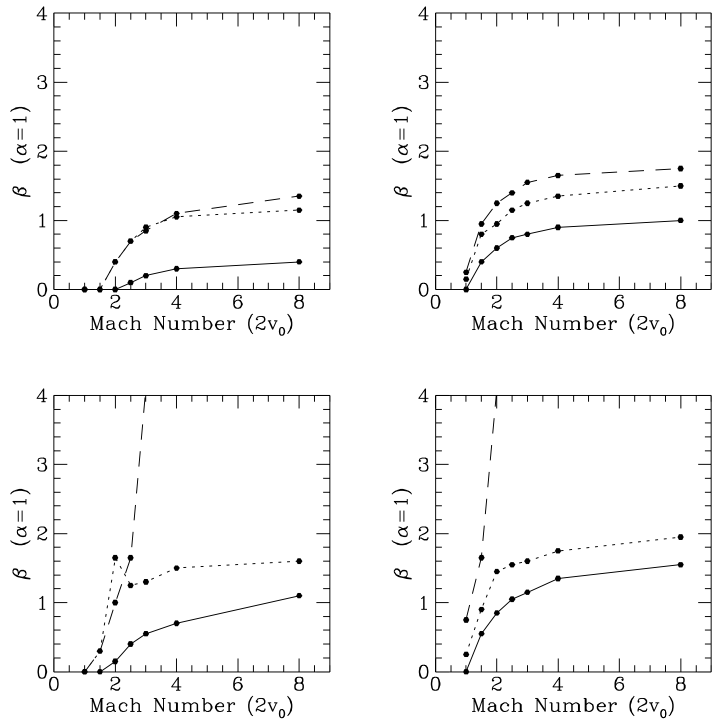

Figure 3.17: Value of β required to stop particle interpenetration from occurring with $\alpha = 1$ for various Mach number shocks in two dimensions. Shown are the adiabatic (top) and isothermal (bottom) shock results, with cubic (solid), unaligned (dotted) and offset (dashed) particle distributions and with constant smoothing lengths of 1 (left) and 1.5 (right) times the initial particle spacing ($h = 0.125$).

is sufficient to damp out most particle oscillations in the post-shock gas. Increasing the value of α to a value of $\alpha = 1$ in these cases only effects the value of β that is required to stop particle interpenetration for shock speeds close to the sound speed, as the β-viscosity provides the main viscous force in halting particle interpenetration in high-Mach-number shocks. This is demonstrated in the two-dimensional calculations in Figure 3.17 where $\alpha = 1$ has been used, varying only β to halt particle interpenetration. Comparing these results with those in Figure 3.15 we find that only in shocks with speeds less than Mach 3 are the values of β required to stop interpenetration affected much by the increased value of α. In cases with the smoothing length equal to the initial particle separation no β-viscosity is required to stop a Mach 1 collision, though some is required for slightly larger smoothing lengths.

Finally, the above simulations all use equal particle densities and equal mass particles on each side of the shock. Other simulations where the two steams are of unequal initial density have also been modelled, with particles on one side of the origin being spaced twice as far apart as on the other side, so giving an 8:1 density contrast across the velocity discontinuity. This was done to see if the particles would find it easier to penetrate into a less dense region. In fact, these simulations require less viscosity than in cases where the particle density is equal in both streams to stop particle interpenetration, as the less dense material is stopped and swept up by the denser material. If unequal mass particles are used, however, these results may change.

3.1.4 Summary of Shock Reproduction and Interpenetration Tests

In conclusion, SPH can give good reproduction of shocks. The quality of the reproduction does not depend on the dimension of the SPH calculations, nor does it depend significantly on the particle distribution, so long as the particles are distributed fairly equally along each dimension and particle interpenetration does not occur. Instead the reproduction of the shock is dependent mainly upon the smoothing lengths of the particles, and hence in the case of variable smoothing lengths, on the particle resolution, as this controls the smoothing lengths. For values of $\alpha = 1$ and $\beta = 2$ the shock is spread over $\approx 3h$, and this increases if the viscosity is increased. If the smoothing lengths are large in comparison to the shock width, the shock is smoothed out and does not attain the correct conditions.

As expected from the formulation of the viscosity, the α-viscosity provides the bulk viscosity in the shock tests, which reduces particle velocity oscillations in the shocked gas, and hence the related oscillations in density and thermal energy. The β-viscosity is ineffective in this regard, and is only important at the edges of the shock where relative particle velocities are close to the sound speed or greater. In general, to provide acceptable bulk viscosity for simulations in which shocks can occur, in one-dimensional SPH a value of $\alpha \gtrsim 0.5$ should be used, while for two and three-dimensional versions $\alpha \gtrsim 1$ should be used. This should give particle-velocity oscillations of no more than a few percent of the sound speed in shocks up to Mach 10 that are well resolved.

In strong shocks in two or three-dimensional SPH where the particle distribution becomes compressed along one dimension, the shock density may be over estimated due to the particles becoming detached from each other and the density being calculated with a multi-dimensional kernel but with a one-dimensional distribution of particles. This cannot be avoided while using a spherical kernel.

In cases where particle interpenetration occurs, there is, of course, significant velocity dispersion of particles in the shock, and also the density is incorrectly calculated. If particles penetrate right through the shock, the shock reproduction breaks down completely.

To stop particle interpenetration in one-dimensional SPH, generally a value of $\beta \gtrsim 1$ should be sufficient in adiabatic and isothermal cases with velocities up to Mach 10. For two, and three-dimensional cases values of $\beta \gtrsim 2$ and $\beta \gtrsim 2.5$ respectively, should be sufficient to stop most particle interpenetration in adiabatic and isothermal shocks up to Mach 10, so long as the problem of compression of the particle distribution which leads to particles being pushed through shocks, and to the smoothing lengths of particles shrinking so that they become detached from particles perpendicular to the shock, do not occur. If these problems do occur, no value of the viscosity is sufficient

Polytrope Index, n	Particle Number	$-E_{\rm T}/E_{\rm G}$
1.0	500	0.513
	4000	0.497
1.5	500	0.512
	1000	0.503
	2000	0.499
	4000	0.497

Table 3.1: Magnitudes of the ratios of thermal to gravitational energies as calculated by the SPH code for each polytrope that is formed. The correct value is 1/2.

to stop interpenetration. To avoid this, care should be taken that particle distributions do not line up along the direction of motion of the shock (as they do with the offset distribution). Instead the distribution should be more 'random' so that passages down which particles could travel are blocked. If it is known that a strong shock will occur in a certain direction, the particles can be spaced further apart initially along that axis so that when compression occurs, the particles do not become detached so easily. An alternative to this is to use non-spherical kernels, however this may lead to unphysical transport of angular momentum and should only be used in special cases (Fulbright et al. 1995).

Finally, the typically recommended viscosity values of $\alpha = 1$ and $\beta = 2$ should generally give good results in three dimensions, and if penetration does occur it should not occur very much, though the value of β could be increased to 3 to give extra insurance against penetration for velocities of around Mach 10. The viscosity used by Lattanzio et al.(1985) of $\alpha = 2$ and $\beta = 4$ for studying cloud collisions should easily stop particle interpenetration in shocks of Mach $\sim$ 10 and indeed much higher, since in theory (it is a second-order viscosity) and as we have observed here, the value of β required to stop penetration for high velocity shocks increases less quickly as the Mach number increases (so long as the particle distribution remains relatively uniform).

3.2 Formation of Polytropes

A simple calculation that tests the interaction of the gravity and hydrodynamic elements of the code is the formation of a hydrostatic, polytropic, gas sphere. The results can be compared directly to theoretical polytrope solutions (Chandrasekhar 1939).

To form the polytropes an initially uniform, isothermal, spherical gas cloud is allowed to collapse under self-gravity using a polytropic equation of state

$$p = K\rho^{\gamma} = K\rho^{(n+1)/n}, \tag{3.7}$$

where in this case, K is kept constant throughout the collapse. When the pressure at the centre becomes large enough to halt the collapse, a central bounce occurs and the cloud oscillates about its equilibrium state slowly damping down to form a polytrope.

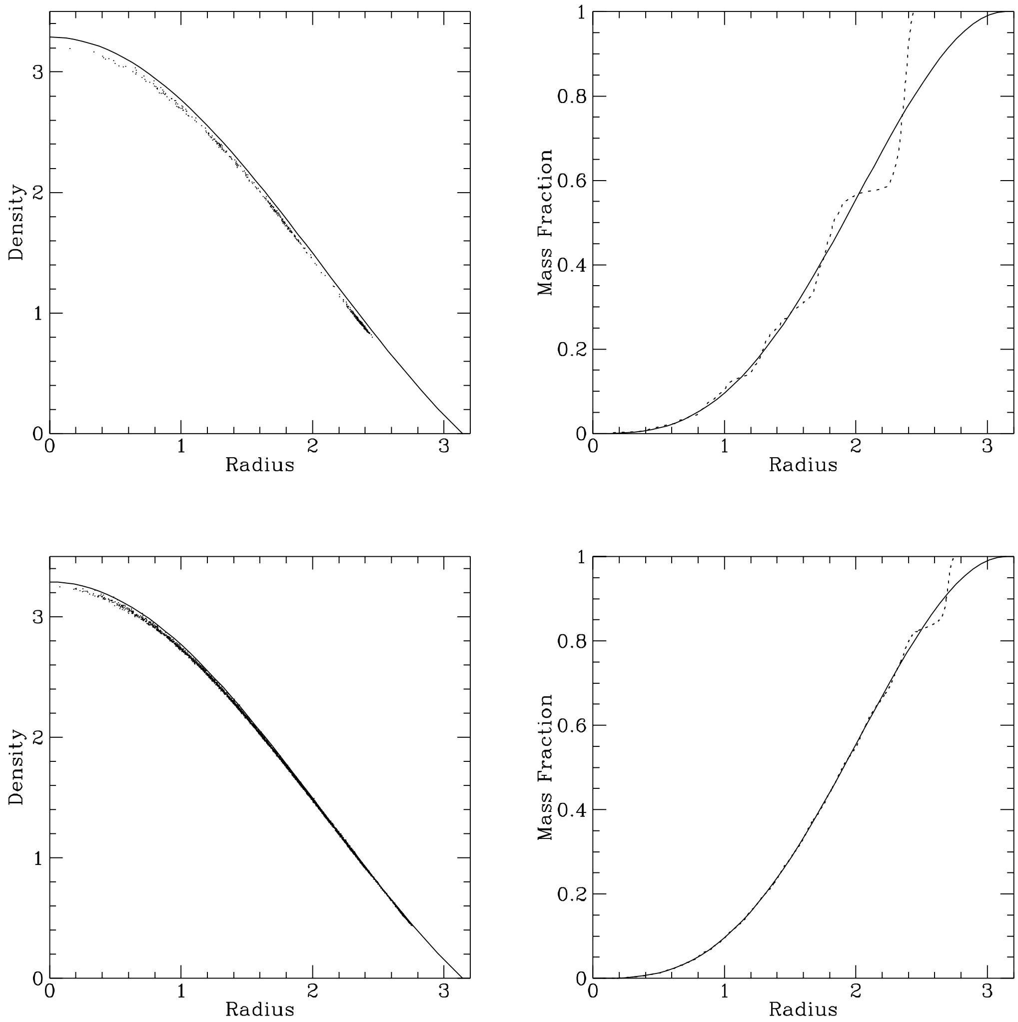

Figure 3.18: The density (left) and mass (right) distributions for $n = 1$ polytropes simulated with 500 (top) and 4000 (bottom) particles. The solid lines are the analytic solutions.

To decrease the magnitude of the post-collapse oscillations and quickly damp them out, strong artificial viscosity of $\alpha = 2$ and $\beta = 4$ is used.

Polytropes of index $n = 1$ ($\gamma = 2$) and $n = 3/2$ ($\gamma = 5/3$) are formed, each with several different numbers of particles. For an $n = 1$ polytrope, the density distribution can be obtained analytically and is given by

$$\rho = \rho_{\mathrm{c}} \frac{sin(\pi r/R)}{(\pi r/R)}, \tag{3.8}$$

where ρ_{c} is the central density, and R is the radius of the polytrope. For the $n = 3/2$ polytrope the SPH results are compared to the density distribution derived from the values tabulated by Fairclough (1932). Figures 3.18 and 3.19 show the SPH density and mass distributions for $n = 1$ and $n = 3/2$ polytropes respectively that are obtained from 500 and 4000-particle simulations. They are compared to the theoretical polytrope solutions. All the SPH results show lower particle densities than expected from theory at the centre of the polytrope. This is because each particle's density is calculated over

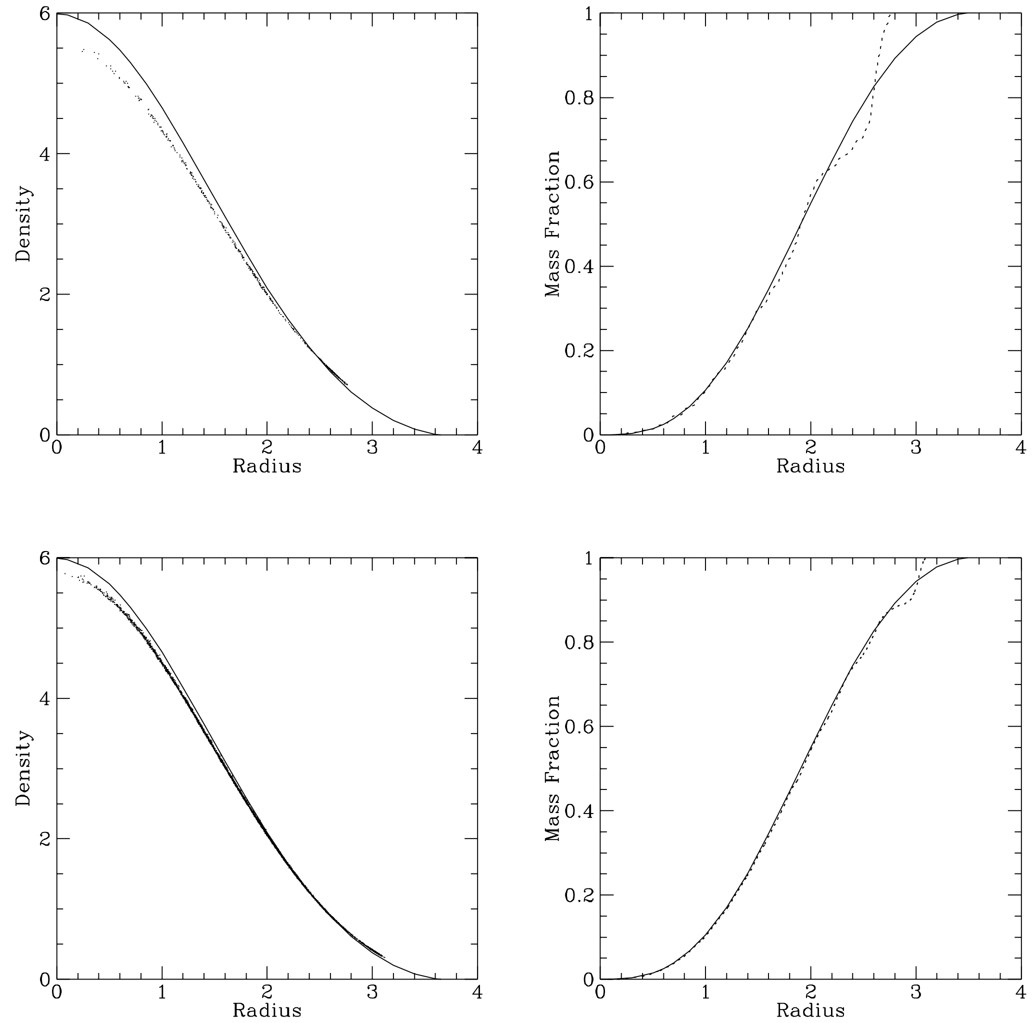

Figure 3.19: The density (left) and mass (right) distributions for $n = 3/2$ polytropes simulated with 500 (top) and 4000 (bottom) particles. The solid lines are the theoretical solutions.

a finite volume, and the density decreases in all directions at the centre. The effect is decreased by increasing the number of particles or, as the difference between the $n = 1$ and $n = 3/2$ polytrope distributions show, by a decrease in density gradient at the centre. Density throughout the rest of the polytrope is modelled well. In particular, the edge effects that appear in the mass distributions due to the discreteness of the simulation and the lower resolution at the edge do not affect the density profiles. In all cases, the particle density dispersion is small as is expected in an equilibrium state.

Table 3.1 gives the magnitude of the ratio of thermal to gravitational energies for each of the polytropes that were formed as calculated by the SPH code itself. The values from the 2000 and 4000-particle simulations are in good agreement with the expected value of 0.5 from the virial theorem. The 500 and 1000-particle simulations give values that are high purely due to the discreteness of the simulation.

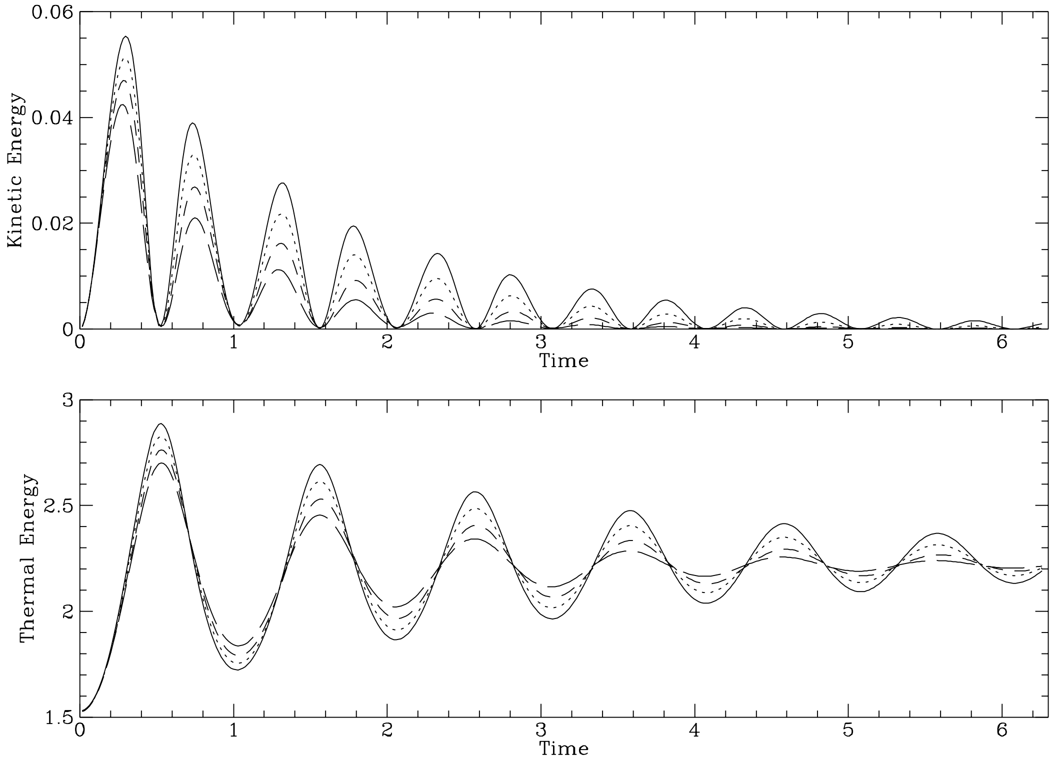

Figure 3.20: Kinetic (top) and thermal (bottom) energies of the oscillating $n = 3/2$ polytropes for 4000 (solid), 2000 (dotted), 1000 (dashed) and 500 (long-dashed) particles, all with artificial viscosity of $\alpha = 1$ and $\beta = 2$. Time is shown in theoretical oscillation periods, with the other units being arbitrary.

3.3 Oscillation of Polytropes

The $n = 3/2$ polytropes obtained in Section 3.2 can be used to investigate damping due to the artificial viscosity, and any inherent damping in the code even with no artificial viscosity. This is done by radially perturbing the polytropes from hydrostatic equilibrium and allowing them to oscillate about their equilibrium state, observing any damping of the oscillations. The initial state consists of a polytrope expanded radially by 20% over the equilibrium configuration. The expected oscillation period is the fundamental radial pulsation period as determined from the linear adiabatic wave equation (Cox 1980).

Oscillations of polytropes with several different numbers of particles and values of artificial viscosity are performed. Figure 3.20 shows the kinetic and thermal energies of the oscillating polytropes with various numbers of particles. It can be seen that reducing the number of particles increases the damping of the oscillations. This is because each particle is smoothed over a larger volume, and hence the viscous forces between particles act over larger distances and over larger velocity dispersions, increasing the bulk viscosity.

Figure 3.21 shows the effect of varying the artificial viscosity. With no artificial viscosity the amplitude of the thermal (and gravitational) energy oscillations decrease, but the kinetic energy oscillations of the polytrope slowly grow. Eventually this results

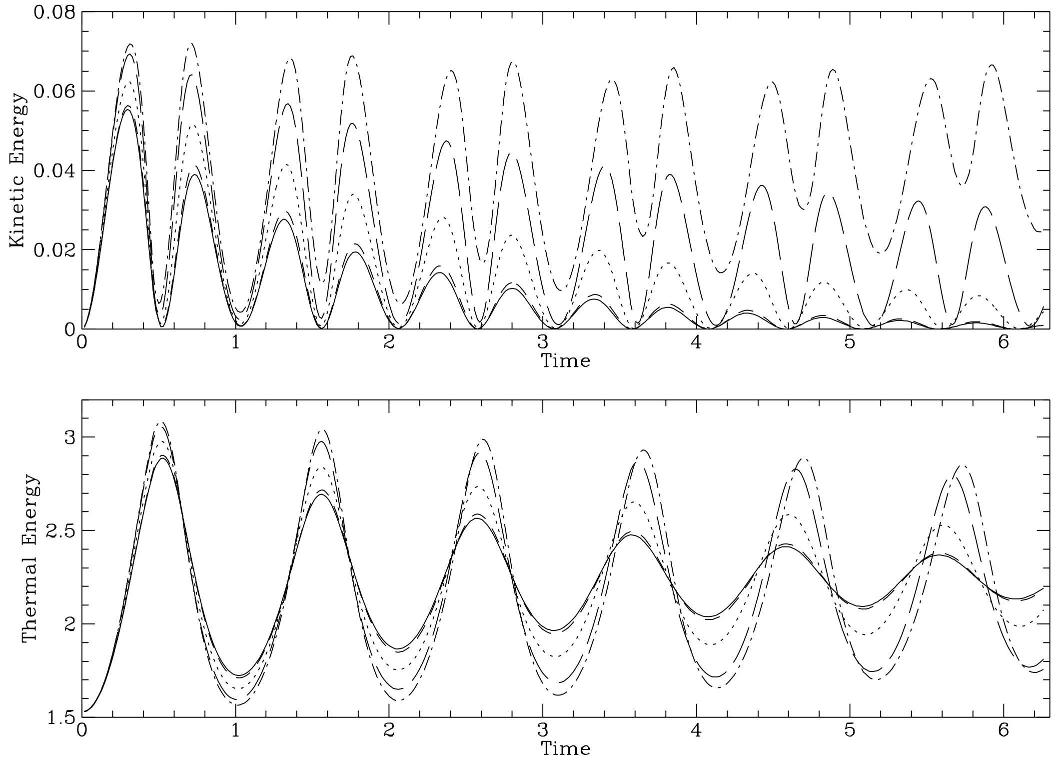

Figure 3.21: Kinetic (top) and thermal (bottom) energies of the oscillating $n = 3/2$ polytropes with 4000 particles, and different artificial viscosities. The viscosities are $\alpha = 1$, $\beta = 2$ (solid), $\alpha = 1/2$, $\beta = 1$ (dotted), $\alpha = 1$, $\beta = 0$ (dashed), $\alpha = 0$, $\beta = 2$ (long dashed), $\alpha = \beta = 0$ (dot-dash). Time is shown in theoretical oscillation periods, with the other units being arbitrary.

in the destruction of the polytrope as noted by Steinmetz and Müller (1992). A very small amount of artificial viscosity is required to make the system numerically stable. With artificial viscosity, damping of the oscillations increases with the viscosity. The difference between the α-viscosity and β-viscosity is clearly seen. As expected, the β-viscosity produces very little damping compared to the α-viscosity, as β-viscosity is only important for high-Mach-number shocks, which do not occur in these calculations.

The periods and Q-factors are listed in Table 3.2. All the oscillation periods are slightly longer than the theoretical period, but they converge to the expected value as the bulk artificial viscosity is increased. The oscillation periods are not dependent on the number of particles used.

Particle Number	α	β	Period	Q
500	1	2	1.011	5.1
1000	1	2	1.016	6.3
2000	1	2	1.013	8.1
4000	0	0	1.034	53
	0	2	1.029	46
	1	0	1.014	10.5
	1/2	1	1.018	18
	1	2	1.013	9.9

Table 3.2: Oscillation periods and Q-factors for the oscillating $n = 3/2$ polytropes. The periods are expressed in units of the theoretical period. The Q-factor is calculated from the thermal energy oscillations as $A_1/A_2 = e^{\pi/Q}$ where A_1 and A_2 are the amplitudes of consecutive peaks.

3.4 Spherical Collapse

A commonly performed test is the collapse of a spherical gas cloud with heating due to shocks. Following Evrard and others (Evrard 1988, Hernquist & Katz 1989, Steinmetz & Müller 1992) the initial state consists of an isothermal spherical gas cloud of mass M, radius R, and density profile

$$\rho = \frac{M}{2\pi R^2}\frac{1}{r} \tag{3.9}$$

The gas has an initial internal energy per unit mass of $u = 0.05GM/R$, with a ratio of specific heats of $\gamma = 5/3$. The ideal equation of state (Equation 2.23) is used with energy conservation (Equation 2.37). As with Evrard the results are given in units of $\rho_* = 3M/4\pi R^3$, $u_* = GM/R$, $v_* = (GM/R)^{1/2}$, $P_* = \rho_* u_*$ and the free-fall time $t_* = (\pi^2 R^3/8GM)^{1/2}$, with $G = M = R = 1$. States of the system shown in the figures are given at times corresponding to Steinmetz and Müller, though their normalisation of time differs by the factor $(\pi^2/8)^{1/2}$ from the above.

The evolution of the system is as follows. Initially the cloud collapses under self-gravity due to the lack of pressure support. The density and pressure rise in the centre of the cloud and the magnitude of the ratio of thermal energy to gravitational energy (initially much less than 0.5) increases. This continues until at some point the pressure gradient becomes large enough to slow down and, eventually stop, the collapse. A central bounce occurs, forming a shock wave that propagates outward. The system then settles down to virial equilibrium, after oscillating for a while.

Several of these collapse simulations are performed varying the strength and form of the artificial viscosity and the number of particles. The results are compared to those obtained using a one-dimensional, spherically-symmetric, Lagrangian, finite-difference code as used by Thomas (1982). The finite-difference code had 5000 equal-mass shells and used the same form of viscosity as Thomas. In the initial SPH simulations, the form and strength of the artificial viscosity is kept constant while varying the number

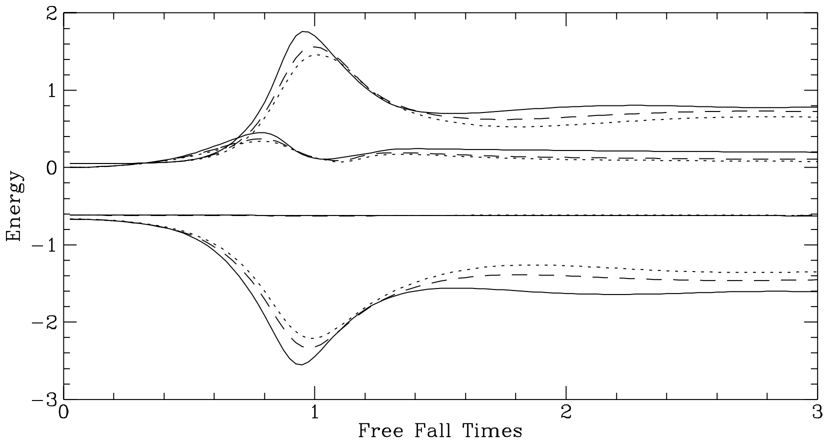

Figure 3.22: Thermal (top), kinetic, total, and gravitational (bottom) energies of the system with the finite-difference code (solid), and 4000 (dotted) and 8000 (dashed) particle SPH simulations. The SPH viscosity used was $\alpha = 1$ and $\beta = 2$.

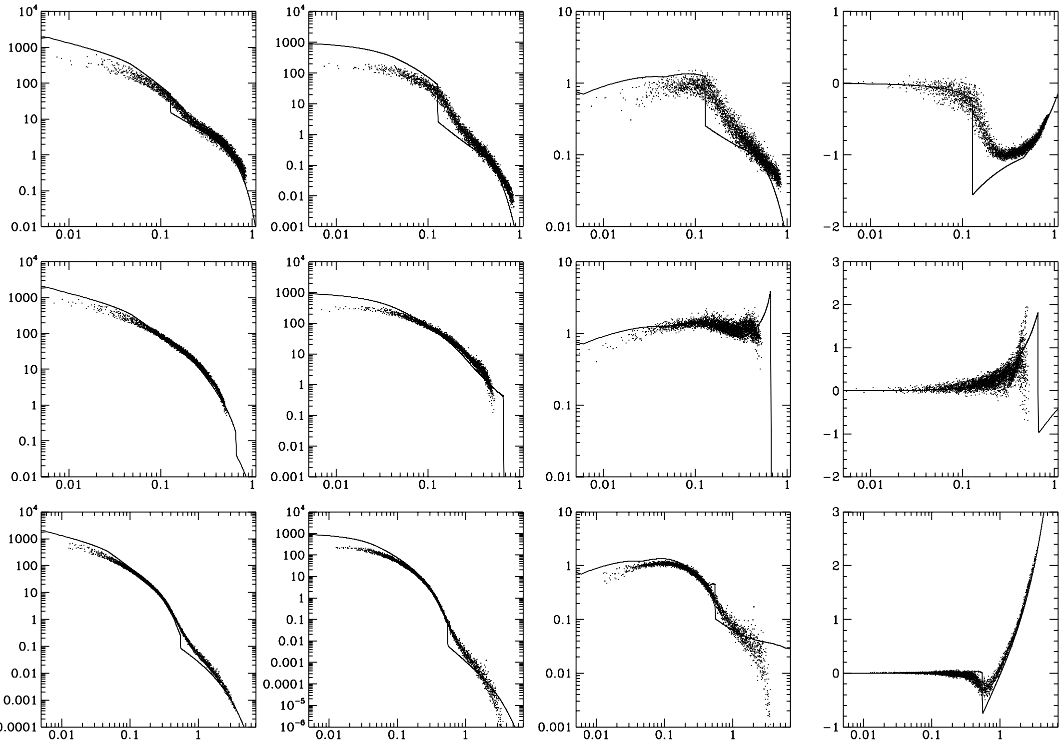

Figure 3.23: Radial density (left), pressure, internal energy, and velocity (right) profiles at times t = 0.70 (top), t = 1.15, and t = 2.33 (bottom) for a 4000-particle SPH simulation as compared to the finite-difference code (solid line). The viscosity was $\alpha = 1$ and $\beta = 2$.

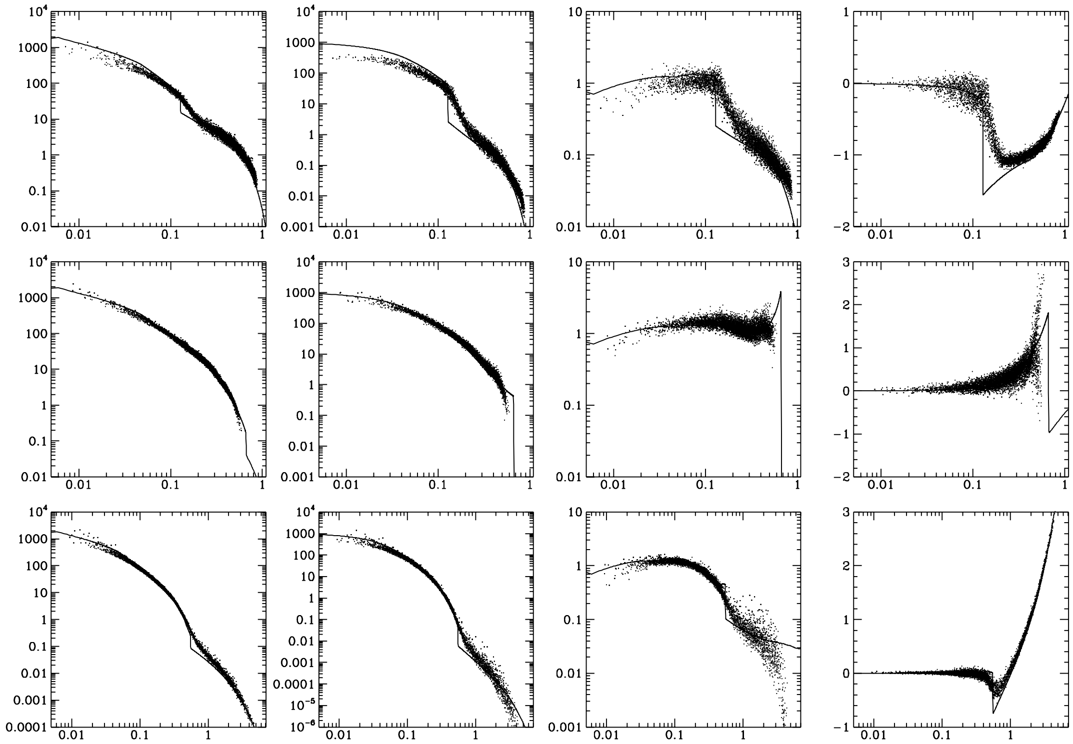

Figure 3.24: Radial density (left), pressure, internal energy, and velocity (right) profiles at times $t = 0.70$ (top), $t = 1.15$, and $t = 2.33$ (bottom) for an 8000-particle SPH simulation as compared to the finite-difference code (solid line). The viscosity was $\alpha = 1$ and $\beta = 2$.

of particles used. Figure 3.22 shows the thermal, kinetic, potential and total energies of the cloud during the evolution for 4000 and 8000-particle simulations compared to the finite-difference code. It can be seen that initially the SPH results compare well with the finite difference code, but at bounce the thermal energy of the system is low and the system has not collapsed to the density that it should have. The situation is improved with increased particle number, and hence resolution. All the SPH cloud collapse simulations conserve total energy to $\leq 1.7\%$. Figures 3.23 and 3.24 show the radial density, pressure, internal energy and velocity profiles at three different times and show why the global energies differ from the finite-difference code. Overall the global behaviour of the system is reproduced by the SPH results. The shock wave is visible and the general states of the system match the finite-difference results. However, the shock wave is lacking in resolution so that the total kinetic energy is underestimated and due to the lower velocities the correct central density is not reached before the bounce occurs, giving lower total thermal energy. The resolution of the shock, and hence global behaviour, is improved in the 8000-particle simulation. These results compare well with Steinmetz and Müller (1992).

Figure 3.25 shows the global energies for several calculations all performed with 4000 particles, but with different artificial viscosities. Reducing the total viscosity from

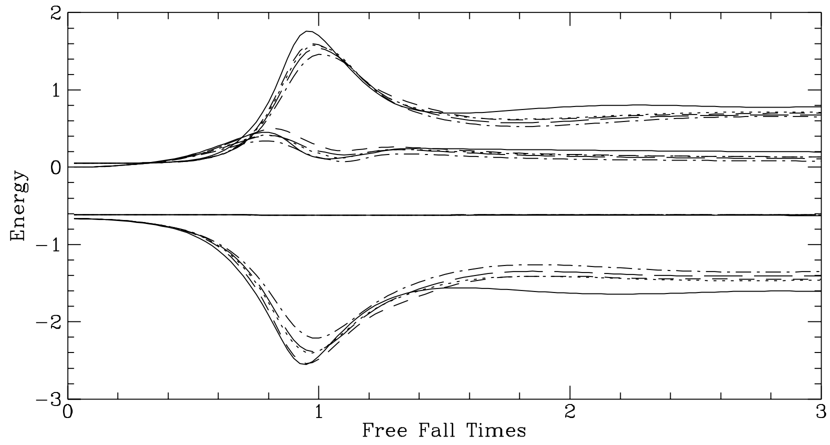

Figure 3.25: Thermal (top), kinetic, total, and gravitational (bottom) energies of the system with the finite-difference code (solid), and 4000-particle SPH simulations with viscosity of $\alpha = 1$, $\beta = 2$ (dot-dash), $\alpha = 0.2$, $\beta = 0.4$ (dashed), $\alpha = 1$, $\beta = 0$ (long-dashed), $\alpha = 0$, $\beta = 2$ (dotted).

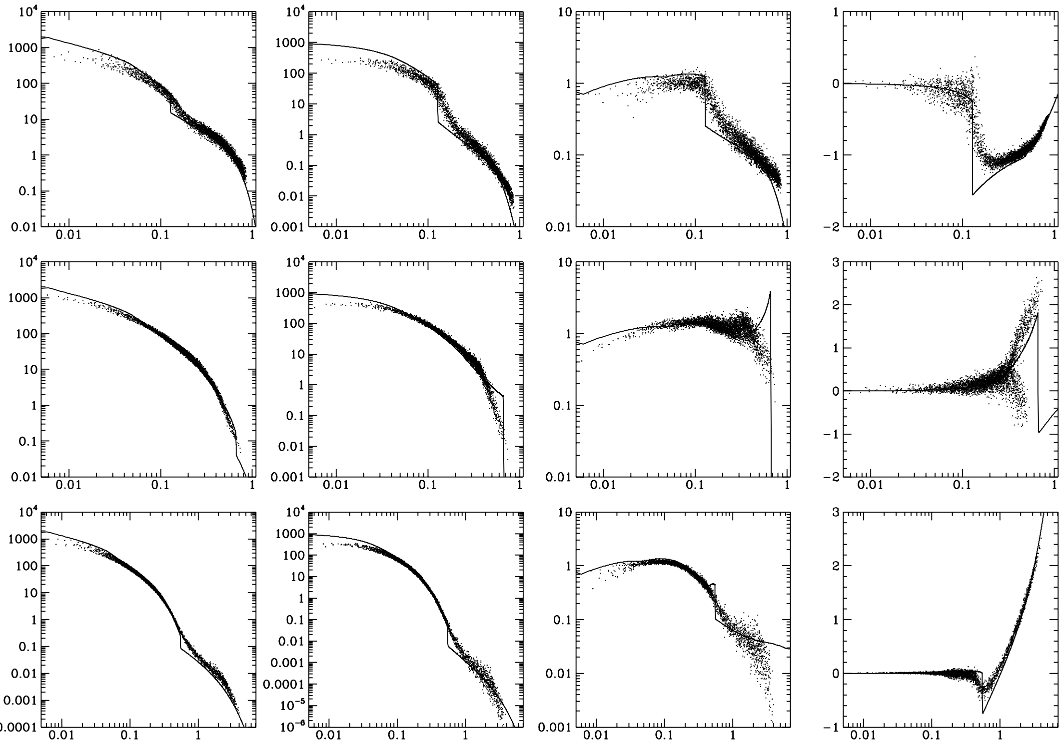

Figure 3.26: Radial density (left), pressure, internal energy, and velocity (right) profiles at times $t = 0.70$ (top), $t = 1.15$, and $t = 2.33$ (bottom) for a 4000-particle SPH simulation as compared to the finite-difference code (solid line). The viscosity was $\alpha = 1$ and $\beta = 0$.

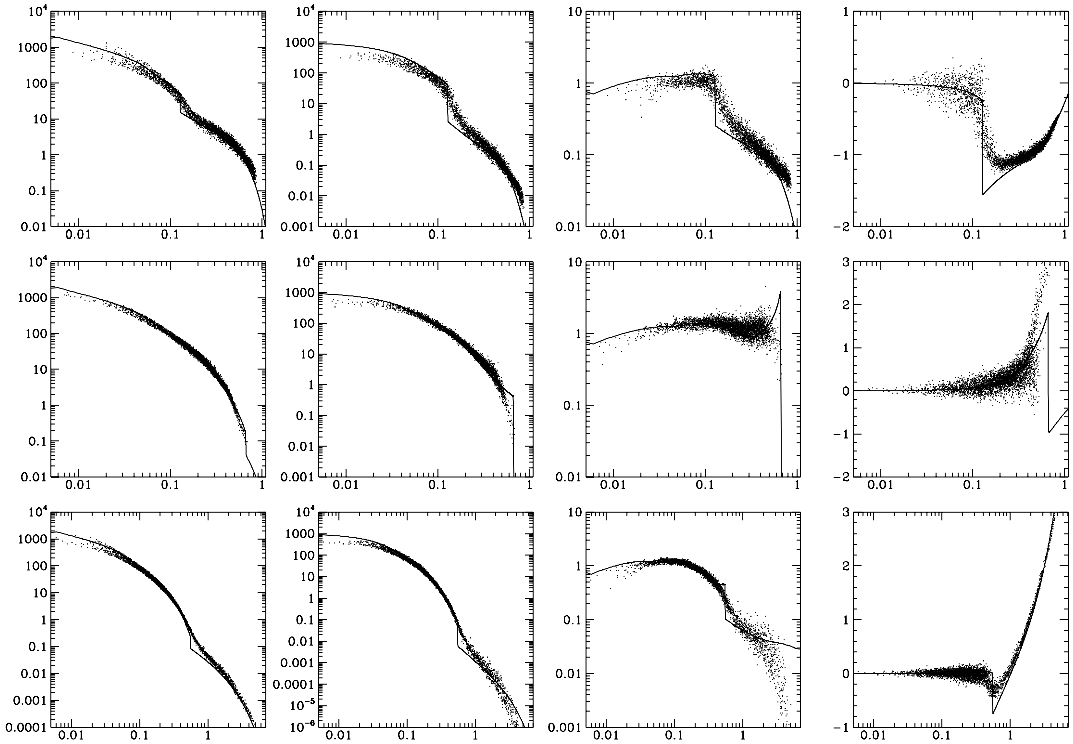

Figure 3.27: Radial density (left), pressure, internal energy, and velocity (right) profiles at times $t = 0.70$ (top), $t = 1.15$, and $t = 2.33$ (bottom) for a 4000-particle SPH simulation as compared to the finite-difference code (solid line). The viscosity was $\alpha = 0$ and $\beta = 2$.

$\alpha = 1$ and $\beta = 2$ increases the kinetic energy before bounce, and hence increases the thermal energy at the bounce and allows the collapse to proceed further before halting it. From this respect the lower-viscosity calculations follow the finite-difference code results better. However, there are other less desirable features. The lower viscosity leads to the bounce being broader since particles take longer to be stopped and re-expand during and after the bounce. This is shown in the kinetic energy of the system at bounce, which is much too high, because the particles have not been stopped and damped due to the lack of viscosity. Note that the two cases with α-viscosity alone ($\alpha = 1$) and β-viscosity alone ($\beta = 2$) have almost identical energies at bounce. This reflects the fact that the system is in the regime where both α-viscosity and β-viscosity are important (i.e. relative particle velocities of order the sound speed).

Figures 3.26 and 3.27 which show system profiles at different times reveal their effects to be quite different, however. The differences are most obvious in the radial velocity plots. At $t = 0.70$, both have resolved the shock much better than the 4000-particle $\alpha = 1$ and $\beta = 2$ simulation in Figure 3.23. However, notice that the velocity dispersion in the calculation with only β-viscosity is much greater than with $\alpha = 1$ and $\beta = 2$, due to the lack of bulk viscosity. The calculation with only α-viscosity has less dispersion than that with only β-viscosity, but at $t = 1.15$ there is obvious particle

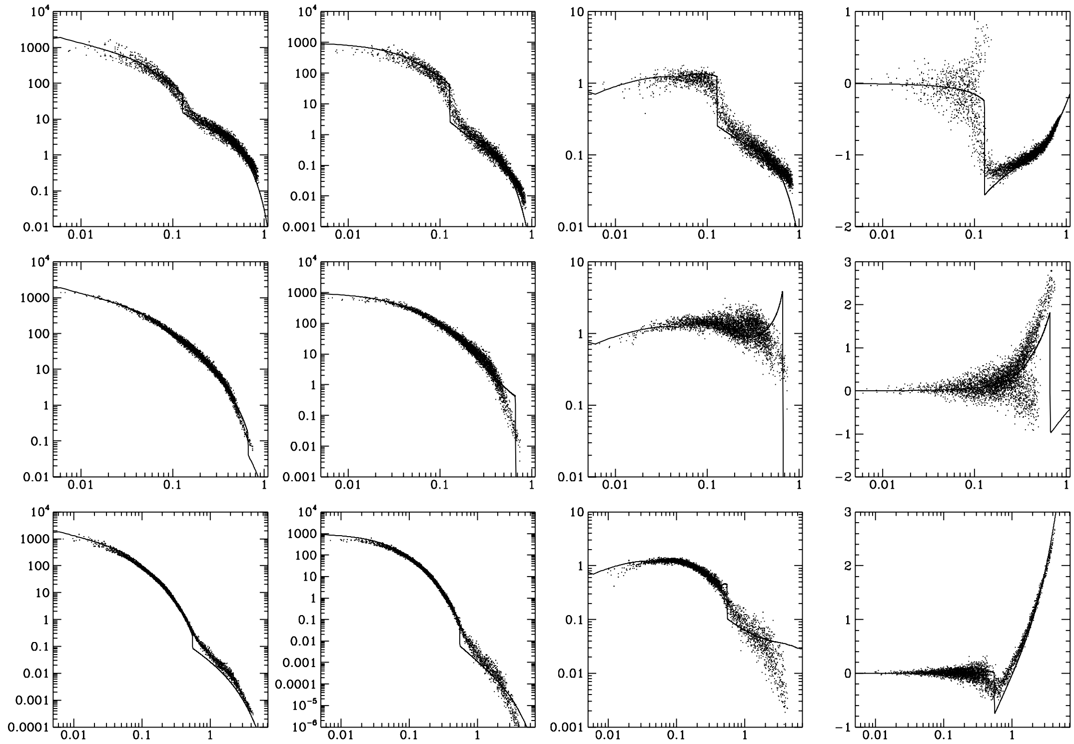

Figure 3.28: Radial density (left), pressure, internal energy, and velocity (right) profiles at times $t = 0.70$ (top), $t = 1.15$, and $t = 2.33$ (bottom) for a 4000-particle SPH simulation as compared to the finite-difference code (solid line). The viscosity was $\alpha = 0.2$ and $\beta = 0.4$.

interpenetration, due to the lack of β-viscosity, between particles that are falling inward from outside the shock and particles that are being forced out by the bounce. Figure 3.28, which shows the profiles of the $\alpha = 0.2$ and $\beta = 0.4$ simulation, has both these problems. The radial-velocity dispersion is very large, and again particle interpenetration occurs at $t = 1.15$. The particle interpenetration is clearly visible in simulations with viscosity of $\alpha = 0.6$ and $\beta = 1.2$ and less. This is a good check of how well viscosity behaves in a real SPH simulation as opposed to the 'artificial' shock tests earlier. From the shock tube tests, it was concluded that if shocks of order the sound speed or more occur, viscosity of much less than $\alpha = 1$ and $\beta = 2$ should not be used. This conclusion is in good agreement with the calculations presented here.